Published in final edited form as:
Free Radic Biol Med. 2007 July 15; 43(2): 300–316. doi:10.1016/j.freeradbiomed.2007.04.015.

Organelle Redox of CF and CFTR-Corrected Airway Epithelia

Christian Schwarzer[1,2], **Beate Illek**[2], **Jung H. Suh**[2], **S. James Remington**[3], **Horst Fischer**[2], and **Terry E. Machen**[1]

[1]Department of Molecular and Cell Biology, University of California-Berkeley, Berkeley, CA 94720-3200

[2]Children's Hospital Oakland Research Institute, Oakland, CA 94609

[3]Institute of Molecular Biology, University of Oregon, Eugene, OR 97403-1229

Abstract

In cystic fibrosis reduced CFTR function may alter redox properties of airway epithelial cells. Redox-sensitive GFP (roGFP1) and imaging microscopy were used to measure redox potentials of cytosol, ER, mitochondria and cell surface of cystic fibrosis nasal epithelial cells and CFTR-corrected cells. We also measured glutathione and cysteine thiol redox states in cell lysates and apical fluids to provide coverage over a range of redox potentials and environments that might be affected by CFTR. As measured with roGFP1, redox potentials at the cell surface (~ -207 ±8 mV) and in the ER (~ -217 ±1 mV) and rates of regulation of the apical fluid and ER lumen following DTT treatment were similar for CF and CFTR-corrected cells. CF and CFTR-corrected cells had similar redox potentials in mitochondria (-344 ±9 mV) and cytosol (-322 ±7 mV). Oxidation of carboxy-dichlorodihydrofluoresceindiacetate and of apical Amplex Red occurred at equal rates in CF and CFTR-corrected cells. Glutathione and cysteine redox couples in cell lysates and apical fluid were equal in CF and CFTR-corrected cells. These quantitative estimates of organelle redox potentials combined with apical and cell measurements using small molecule couples confirmed there were no differences in redox properties of CF and CFTR-corrected cells.

Keywords

redox-sensitive green fluorescent protein; cystic fibrosis; mitochondria; endoplasmic reticulum; cell surface; organelle redox potential

Introduction

A number of studies have indicated that redox balance in the airways may be altered in CF and that this may contribute to inflammatory properties of the epithelial cells. *In vitro*

Address for correspondence: Terry E. Machen Dept of Molecular and Cell Biology 231 LSA University of California-Berkeley Berkeley, CA 94720-3200 Tel: 510-642-2983 Fax: 510-643-6791 tmachen@berkeley.edu.

experiments have suggested that CFTR may be involved in maintaining the redox status of the ASL, and that a mutation in CFTR could impair lung antioxidant defenses, thereby making the CF lung more susceptible to oxidative stress (1,2,3,4). Because oxidative stress can activate NF-ĸB (5), similar oxidative imbalance in the lungs of CF patients (6) could lead to hyper inflammatory responses from the airway epithelial cells (7).

WT-CFTR conducts reduced glutathione (GSH, see 8), a key redox buffer in cells. Cells containing defective CFTR secrete less GSH than control cells containing functional CFTR, and transfection of these cells with functional CFTR restored GSH secretion to control levels (1). Further, BAL fluids from CFTR-knock out mice had decreased concentrations of GSH and increased concentrations of other indicators of oxidative stress. However, tissue concentrations of GSH were similar, and the activities of glutathione reductase and glutathione peroxidase were increased, whereas the activity of γ-glutamyltransferase was unchanged (7). Although these latter data were consistent with the hypothesis that CFTR may be involved in redox homeostasis of the ASL, it is difficult to determine whether these changes resulted from the absence of functional CFTR or from the accompanying infection and infiltration of leucocytes that produce ROS. Loss of CFTR-mediated GSH conductance might be particularly important to CF pathophysiology since recent experiments have demonstrated that Duox 1, a H_2O_2- generating member of the NADPH oxidase family, is expressed in the apical membranes of airway epithelia (9), which might then lead to over oxidation of the airway surface liquid (ASL).

Another potential contributor to altered redox balance in CF is the activity of mitochondria. Based on finding low O_2 concentrations in fluids bathing airway epithelial cells, it has been proposed that both the airway surface liquid and the cells are hypoxic in CF (10), resulting from upregulated ENaC (11, 12) and increased ATP consumption by the Na^+/K^+-ATPases in the basolateral membranes of the cells (13) and increased O_2 consumption (14). Because hypoxia can lead to increased production of ROS by mitochondria (15, 16), it might be expected that this effect would oxidize the mitochondrial matrix in CF cells compared to normal. Recent experiments have shown substantial reductions in glutathione levels measured in mitochondria and cytosol from CF cells, indicative of excess oxidation in CF (17).

Finally, it has been proposed that accumulation of ΔF508CFTR in the endoplasmic reticulum (ER) leads to altered Ca^{2+} permeability and signaling (18), and it seemed reasonable that this perturbation in Ca^{2+} regulation of the ER might also be associated with alterations of the redox status of the ER, which is thought to be highly oxidized (19).

Based on these data we initiated a study of the potential role of CFTR in controlling redox balance in airway epithelial cells. We utilized the newly described ratiometric, redox-sensitive GFP1 (roGFP1, 20; 21) to measure redox potentials. roGFP1 was genetically targeted to the cytosol, endoplasmic reticulum (ER), mitochondria and apical surface in the CF nasal epithelial cell line CF15 (22), a cell line that is homozygous for the deletion of phenyl alanine 508 (ΔF508) and exhibits amiloride-sensitive Na^+ transport but no forskolin-activated Cl^- secretion (23; 24). Quantitative measurements of roGFP1 fluorescence were

performed using ratio imaging microscopy on living cells including calibrations of the fluorescence signals in terms of redox potentials.

These real time, quantitative measurements were compared to measurements using other approaches that are less quantitative but provide sensitive assays of small changes in redox. The redox-sensitive probe Amplex Red was used to assess redox properties of the fluid bathing the apical surface of these cells for comparison to measurements of surface-targeted roGFP. The redox probe carboxy-dichlorodihydrofluoresceindiacetate was also used to assay cytosolic redox properties and to compare to those obtained with the cytosolic roGFP. Finally, HPLC was used to measure oxidized and reduced forms of glutathione and cysteine in cells and in the liquid bathing the apical surface of CF15 cells. Similar measurements were then also made in cells in which CFTR had been expressed using an adenovirus. In some cases measurements were also made in HeLa cells for comparison to previous work (20, 21).

Methods

Plasmids

Using a plasmid coding for cytosolic roGFP1 (20) as a template, a mitochondrial roGFP1 was generated by cloning the roGFP1 cDNA downstream of the pyruvate dehydrogenase E1α subunit leader sequence (20). A cell surface roGFP1 was generated by cloning the PCR-amplified roGFP1 cDNA into a plasmid derived from pCDNA3 (Invitrogen) coding for a 5'- $CD8^+$ signal sequence (kind gift from H.P. Moore) and adding a PCR-amplified sequence coding for a Gpi anchor of human folate receptor at the 3'-end. An endoplasmic reticulum roGFP1 was generated by cloning the roGFP1 cDNA between a $CD8^+$ signal sequence and the ER retention signal KDEL. The following primer sequences were used to PCR-amplify the cell surface-targeted roGFP1 (roGFP-forward: 5'-gacaagcttatggtgagcaagggcgag-3', roGFP1 reverse: 5'-cagcgggatccgtcttgtacagctcgtcc-3', folate forward: 5'-aagacggatcccgctgcagccatgagtggg-3' and folate reverse: 5'-gtttgcggccgctcagctgagcagccacag-3' for the 3'-Gpi anchor) and the ER-targeted roGFP1 (roGFP1 forward and ER-KDEL reverse: 5'-ggtgggatccttacagctcgtccttgtacagctcgtccat-3'). Cloning was controlled by DNA sequencing.

Cell cultures, transfection and infection procedures

JME/CF15 nasal epithelia cells homozygous for ΔF508 CFTR (termed "CF15" throughout the manuscript) were cultured as described previously (22,24,25). For measuring redox potential using digital imaging microscopy cells were seeded on cover slips, transfected (Effectene, Qiagen) with plasmids coding for each roGFP. To avoid co-transfection by different plasmids into the same cell separate transfection reactions were performed for each plasmid, and cells were trypsinized and reseeded on the same cover glass. Alternatively, transfection cocktails were first mixed separately for each plasmid and then added subsequently to one cover glass. When using this approach, organelle-specific roGFP1-fluorescence in CF15 cells was analyzed carefully before starting the experiment since, while about 50 % percent of the cells appeared to be transduced with only one plasmid, the other 50% of cells exhibited expression of multiple organelle-coding roGFP1 plasmids. In

this situation, we used multiple characteristic identifiers to assure cells were expressing only one, specific subcellular-targeted sensor: Cyto-roGFP1 showed uniform fluorescence throughout the cell including the nucleus. Mito-roGFP1 showed distinct fluorescence puncta in the cytosol but not in the nucleus, and the fluorescent puncta moved in a discontinuous fashion, likely along microtubules. ER-roGFP1 fluorescence showed a uniform reticular staining that did not move, and there was no fluorescence in the nucleus. Surface-roGFP1 labeled only the cell membrane. Cells were monitored for >5 minutes to assure organelle-specific roGFP1 expression.

CF15 cells grown on cover glasses or filters were infected by incubation with adenoviruses (stock 10^{10} pfu/ml; 100 MOI) expressing either CFTR or lacZ (purchased from U. Iowa Vector Core), EGFP (gift from Joseph Zabner, U. Iowa) or CFTR-EGFP (from James M. Wilson, University of Pennsylvania) during 12 hr treatment followed by washing and further 24-48 hr incubation in culture medium. Cells on filters were incubated with adenoviruses in both apical and basolateral solution. The adenovirus-infected cells were termed CF15-CFTR, CF15-lacZ or CF15-EGFP throughout. Infection efficiency of CF15 cells was confirmed by Xgal staining for β–galactosidase expression. Ad-lacZ-infected cells were fixed, incubated with 1 mg/ml Xgal for 18 hrs at 37° C, and examined with a light microscope. Fluorescence of CF15 cells infected with Ad-EGFP was monitored on a confocal microscope (see below) 24 hours post infection.

Immunofluorescence

Confocal microscopy was used to analyze the differentiation of CF15 cells and to study the localization of organelle-targeted roGFP1. To confirm cell differentiation the expression of the tight junction protein zonula occludens 1, ZO-1 (see 26), was used as a marker of epithelia polarization. Cells grown on permeable support were fixed with 4% paraformaldehyde-PBS, washed with PBS and incubated with 1% BSA-PBS. CFTR-GFP adenovirus was used to study CFTR localization in non-fixed CF15 cells 24 hours post infection. Cells were analyzed on a Solamere spinning disc confocal microscope with excitation at 488 nm after immunostaining using a monoclonal anti ZO1 antibody (BD Biosciences, Rockville, MD) and an AlexaFluor 594-conjugated goat anti mice secondary antibody (Invitrogen, Carlsbad, CA). Localization of organelle-targeted roGFP1 was analyzed by bathing living CF15 cells expressing cytosolic, mitochondrial, ER and cell surface roGFP1 in Ringer's solution with 500 μM DTT to increase fluorescence intensity for excitation at 488 nm. Images were obtained using a 515 nm long pass emission filter and a 60× objective.

Redox potential measurements using roGFP1 and imaging microscopy

roGFP-expressing cells were mounted in a chamber on the stage of a Nikon Diaphot microscope. Ratiometric imaging was performed using a CCD camera, filter wheel (Lambda-10, Sutter) and Axon Imaging Workbench 4 (Axon Instruments) to collect emission (>510 nm) images during alternate excitation at 385±5 nm and 474±5 nm. Images were background subtracted, and normalized data were calibrated using roGFP1 ratio values obtained from an *in situ* calibration curve obtained by titrating cells with standard solutions containing varying ratios of DTT_{red} and DTT_{ox} in Ringer's solution at pH 7 and 20 °C. The

redox potential for each of these standard solutions was calculated according to the Nernst equation (eq. 1):

$$E' = E'_{0(DTT)} + RT/nF \times ln\left([DTT_{ox}] / [DTT_{red}]\right) \quad (1)$$

$E'_{0(DTT)}$ = - 0.330 V, at pH 7 and room temperature, R is the gas constant (8.315 $J \cdot K^{-1} \cdot mol^{-1}$), T is the absolute temperature (293 K), n is the number of transferred electrons (2), and F is the Faraday constant ($9.649 \cdot 10^4$ $C \cdot mol^{-1}$).

The *in situ* calibration curve was generated by first preparing the standard solutions consisting of *trans*-4,5-dihydroxy-1,2-dithiane (termed DTT_{ox}) and DL-dithiothreitol (termed DTT_{red}) under nitrogen atmosphere to exclude oxidation by air. Then roGFP1-expressing cells were permeabilized by adding 1 to 5 μg/ml digitonin for 5 to 10 minutes. In separate experiments this procedure permitted propidium iodide (PI, MW = 668) to permeate the membranes (as seen by uptake of PI into the nucleus – not shown) while cytosolic roGFP1 (MW = 28,000) was retained inside the cells. The permeabilized cells were then perfused with different DTT standard solutions covering redox potentials from -330 mV to -195 mV, and 385/474 nm excitation ratios were recorded. The roGFP1 excitation ratios were normalized to the values measured using 10 mM DTT_{red} as 0% oxidation and 10 mM H_2O_2 as 100% oxidation, and the normalized ratios were plotted against the calculated redox potentials of the DTT standard solutions. roGFP1 ratios of 8 different titration experiments were plotted against redox potentials of DTT standards, and data were fit by non linear regression (f= y0+a/(1+exp(-(x-x0)/b)), SigmaPlot 8.0) to generate a curve that was then used for calibrating future experiments.

To test for organelle-specific responsiveness of roGFP1, intact cells expressing the probe in the cytosol, ER, mitochondria and cell surface were treated with solutions containing different concentrations of membrane-permeable DTT_{red} and H_2O_2. These solutions were perfused over the cells, and corresponding roGFP1 385/474 ratios were measured in each of the compartments. Organelle roGFP1 properties from six independent experiments were then compared by plotting raw, background-subtracted 385/474 ratios and normalized 385/474 ratios recorded in 10 mM DTT_{red}, 6 mM DTT_{red}: 2 mM H_2O_2, 2 mM DTT_{red}: 8 mM H_2O_2 and 10 mM H_2O_2.

At the end of each experiment roGFP1 385/474 ratios were recorded during maximal oxidation by treatment with 10 mM H_2O_2 and maximal reduction by treatment with 10 mM DTT, and these maximal and minimal roGFP1 385/474 ratios were then used in combination with the above mentioned *in situ* calibration curve to calculate redox potentials measured in each experiment. The percentage of maximum reduction was also reported to allow comparison to previously published fluorescence properties of roGFP1 (20,21).

Because thiol redox reactions necessarily involve H^+ (27), determination of redox potentials in organelles requires knowledge of the pH of the organelles so that the appropriate corrections can be made to the calibration of roGFP1 fluorescence. There is a long history of research attempting to find differences in pH of the Golgi and other organelles in CF vs. non-CF cells, so we considered the possibility that such differences might be relevant for the

calculations here. Chandy *et al* (28) showed cytosolic pH was insignificantly different (pH 7.5-7.6) between CFT1 and CFTR-corrected CFT1 cells using Hepes-buffered solutions (absence of CO_2 and HCO_3 in the media). Similar measurements have been performed in this lab using CF15-lacZ and CF15-CFTR cells. CF15-lacZ cells had pH 7.45+/- 0.10 (18 expts) while CF15-CFTR cells had pH 7.41 +/- 0.20 (10 expts) in solutions containing CO_2/HCO_3 (29). Thus it seems pH of the cytosol is the same in CF and CFTR-corrected CF airway epithelia, and we assumed pH of cytosol was 7.4 and applied the correction of -23.3 mV.

As shown by both us (30, 31) and Grinstein (32, 33), pH of the ER always equals that of the cytosol because the ER has very large H permeability (30, 31) so that pH of the ER is regulated by the transporters present in the plasma membrane. Because pH of the cytosol is the same in CF and CFTR-corrected cells, it therefore seems likely that pH of the ER of the CF and CFTR-corrected cells will also be the same. We therefore applied the same pH correction of -23.3 mV as the cytosol to the ER values.

Mitochondrial pH has not been measured in airway epithelia, but given the similar pH values in the cytosol of CF and CFTR-corrected cells, there is good reason to assume pH in the mitochondria will also be similar in CF and CFTR-corrected cells. In addition, unpublished measurements have shown that, unlike some cells (11, 12), Na^+ transport was not increased in CF15 cells compared to CF15-CFTR cells (Illek, B, and Machen, T.E., unpublished observation), indicating that increased energy consumption may not be a universal outcome in CF airway epithelia. We therefore assumed that mitochondria have pH_{mito} = 8 in both CF15 and CF15-CFTR cells, and this correction (-58.2 mV) was added to values from calibrations obtained at pH 7.0.

For the cells bathed with well buffered pH 7.4 bathing solutions, it is assumed that pH at the cell surfaces is the same as that in the bulk solution, so this correction is -23.3 mV.

In some experiments initial rates of oxidation or reduction in different organelles following addition or wash-out of H_2O_2 or DTT were calculated by plotting redox potentials vs. time and fitting data by linear regression. These rates (mV/s) were calculated over similar redox potential ranges in each case. To estimate the redox potential of the ER and at the cell surface, roGFP1 fluorescence ratios were recorded by titrating cells with 10 to 1000 μM DTT_{red}. Calibrated potentials were plotted vs. [DTT_{red}], and data were then fitted by logarithmic regression (y=a*ln(x)+y0). The intercept y0 correspond to 0 μM DTT_{red} and was used to give an estimate for the redox potential in the ER and at the cell surface. Data from cells treated with [DTT_{red}] = 0 or 1μM were omitted from the fit because roGFP1 ratios appeared to be saturated.

Oxidation of apical Amplex Red and of cytosolic carboxy-H_2 DCFDA

The Amplex Red reagent (10-acetyl-3,7-dihydroxyphenoxazine) and horse radish peroxidase (HRP) were used to measure rates of accumulation of H_2O_2 in the apical solution of CF15 cells grown to confluency on permeable supports and infected with either Ad-lacZ or Ad-CFTR (100 MOI apical and basal). In the presence of HRP, the Amplex Red reagent reacts in a 1:1 stoichiometry with H_2O_2 to produce fluorescent resorufin, which is then assayed

using a fluorescent plate reader (ex: 530 ± 20 nm, em: 590 ± 10 nm) (Wallac Victor Multi Label Counter, Perkin Elmer, Shelton, CT). Assays were performed on the apical solution of the filter-grown cells 48 hrs after adenoviral infection. 50 μM of Amplex Red reagent and 0.1 U/ml of HRP were added to 500 μl of PBS solution on the apical surface of the filter-grown cells, and fluorescence was measured every 5-7 mins for a total of 40 mins. Data were calibrated to a standard curve generated from serial dilutions of H_2O_2 in the HRP-Amplex Red-containing solution, and rates of H_2O_2 production (pmole $\cdot$ cm^{-2} $\cdot$ $h^{-}1$) in the apical solution were calculated by plotting fluorescence data *vs* time and calculating the slope of the curves. Each experimental condition was performed in quadruplicate.

Carboxy-dichlorodihydrofluoresceindiacetate (carboxy-H_2DCFDA) is a cell-permeant indicator for ROS that is nonfluorescent until oxidation occurs within the cell. Similar to the Amplex Red experiments, CF15 cells were grown to confluence on permeable supports and then incubated with 5 μM carboxy-H_2DCFDA on the apical surface. Fluorescence (ex: 490 nm; em: 520 nm) of the resulting cellular DCF was measured in the fluorescence plate reader once every 7-20 mins over the course of 45 mins, and rates of increase of fluorescence were compared for CF15-lacZ- and CF15-CFTR cells. Each experimental condition was performed in six separate cell samples.

LC/MS/MS detection of GSH, GSSG, cysteine and cystine

Intracellular and extracellular GSH and GSSG were detected using LC/MS/MS following derivatization with isopropylchloroformate based on methods previously published by Husek et al (34) with the following modifications (Suh, *et al.*, manuscript in preparation). An aliquot of culture media and cell pellets (1×10^6 cells) were mixed with equal volume of 10 % perchloric acid (PCA) containing 1 mM DTPA. From these samples, the acid-soluble supernatants were collected following centrifugation at 14,000 rpm for 5 min. To the acidified supernatants, homoglutathione (10 μM) was added as an internal control. Subsequent to the addition of internal standards, solid phase extractions with a strong cation exchange resin (phenomenex) were performed to further enrich GSH and GSSG. GSH and GSSG were eluted by treating with 100 μl elution buffer consisting of 0.1 N NaOH, 40% N-propanol, and 10% pyridine. The eluted samples were mixed with 50 μl of derivatizing solution consisting of isooctane, chloroform, and isopropylchloroformate (75:40:10) and allowed to react for 2 min. The derivatized products were subsequently extracted with 200 μl of isooctane and dried under a constant stream of nitrogen. These samples were reconstituted with mobile phase consisting of methanol and water (80:20, v/v). Chromatographic separation of GSH, GSSG, cysteine, cystine, cystine, cystine (3,3,3’3’-D_4) and homoglutathione were performed on C18 reversed-phase column (25 × 2 mm, 0.3 μm) from Phenomenex (Torrance, Ca). The chromatographic system was Shimadzu LC-10AV separation module. The separation was performed under isocratic condition at a flow rate of 0.2 ml/min. Electrospray tandem mass spectrometric analysis was performed on Quattro Micro mass spectrometer from Micromass and analyzed using Masslinks software (3.1 version). Analytes were detected using the multiple reaction monitoring (MRM) scanning mode. Capillary voltage was set to 3 kV, source temperature to 150 C and nebulizer gas temperature to 400 C. The cone and evaporation gas flows were set at 200 and 800L/hr, respectively. Cone voltages for GSH, GSSG, cysteine, cystine, cystine (3,3,3’3’-D_4) and

homoglutathione were set 35, 58, 30, 37, 37 and 35 V, respectively. Collison energy for GSH, GSSG, cysteine, cystine, cystine (3,3,3'3'-D_4) and homoglutathione were all set at 20, 20, 12, 17, 17, and 20 e, respectively. Mass transition pairs monitored for GSH, GSSG cysteine, cystine, cystine (3,3,3'3'-D_4) and homoglutathione derivatives were 564.5>162.2, 953.5>836.5, 336.5>190.3, 497.5>248.5, 501.5>250.5and 578.5>162.2. Homoglutathione and cystine (3,3,3'3'-D_4) were used as internal standards for quantification of GSH/GSSG and cysteine/cystine redox couples. Absolute concentrations were calculated relative to cell number and a cell volume (4 μl per cell (35)) or volume of the apical solution (36) and ratios of each redox couple were converted to redox potentials using Nernst equation (see above).

Measurements of CFTR Cl transport function using the Ussing assay

For short-circuit current (I_{sc}) measurement filter-grown CF15 monolayers were mounted in Ussing chambers. Short-circuit current was recorded as described previously (37). At 20- or 50-s intervals, transepithelial voltage was clamped from 0 to 2 mV, and the transepithelial resistance (R_{te}) was calculated: $R_T = 2\ mV/\Delta I_{SC}$. Cells were treated with apical amiloride (10μM) to block ENaC. A serosa-to-mucosa-directed Cl gradient was applied to amplify CFTR-dependent currents. The serosal Ussing chamber solution contained (in mM) 120 NaCl, 20 $NaHCO_3$, 5 $KHCO_3$, 1.2 NaH_2PO_4, 5.6 glucose, 2.5 $CaCl_2$, and 1.2 $MgCl_2$. In mucosal Ussing chamber solutions, all Cl salts were exchanged for gluconate salts.

Results

Organelle-targeted redox-sensitive GFP (roGFP1)

CF15 cells were transiently transfected with organelle-roGFP1 coding plasmids, and localization of roGFP1 expression was monitored by confocal microscopy. Confocal images in Fig. 1 show the subcellular localization of roGFP1 targeted to the cytosol (Fig. 1A), mitochondria (Fig. 1B), ER (Fig. 1C), and the extracellular cell surface (Fig. 1D) of CF15 cells. Cytosolic roGFP1 was found throughout the cytosol and also in the nucleus. Mitochondrial roGFP1 showed predominantly a tubular staining characteristic for mitochondria oriented along microtubules, and no fluorescence was detected in the nucleus. ER-roGFP1 showed a stable, lacy, network-like, reticular staining throughout the cell, also with no expression in the nucleus. Surface roGFP1 was expressed mainly at the extracellular surface of the plasma membrane but some vesicular-type expression was also detected inside the cell. Mitochondria appeared to move in punctuate fashion over time, while roGFP1 in the other compartments appeared relatively static. These confocal images confirmed organelle-specific expression for each of the four compartments. Cells showed normal morphology compared to non-transfected controls and expressed roGFP1 over the period of about five days.

Comparison of responses of roGFP1 targeted to cytosol, ER, mitochondria and cell surface

Responsiveness of roGFP1 in the cytosol, ER, mitochondria and cell surface of CF15 cells to alterations of redox potential was tested by performing an *in situ* calibration of roGFP1. roGFP1-transfected cells were treated with 1 to 5 μg/ml digitonin for 5 to 10 minutes to permeabilize cell membranes, and cells were then perfused with solutions containing

different DTT_{red}:DTT_{ox} (total concentration of DTT_{red} + DTT_{ox} ≥ 10 mM) while measuring 385/474 nm ratios of roGFP1. Results from a typical experiment are shown in Fig. 2A, which plots cytosolic roGFP1 ratio (solid line) measured with the imaging microscope as a function of time during incubation with DTT standard solutions. Standard solutions permeant through the digitonin-permeabilized cell membrane and provide a convenient way to alter cellular redox potentials. Cells were first treated with 10 mM DTT_{red}, which led to complete reduction of cytosolic roGFP1 (21). When the bath was changed sequentially to DTT standard solutions that had more oxidized redox potentials, the roGFP1 385/474 nm ratio increased and plateaued within 5 to 10 minutes indicating equilibrium with the bath solution. Maximum oxidation was achieved by adding 10 mM H_2O_2 at the end of the experiment. Average steady state roGFP1 fluorescence ratios recorded from eight similar experiments (Fig. 2A) were plotted vs. redox potentials (Fig. 2B) and fitted by nonlinear regression. The resulting *in situ* calibration curve (solid line) had a similar slope but slightly more oxidized midpotential (-276 vs. -288 mV) compared to the *in vitro* calibration curve for isolated recombinant roGFP1 described by Hanson and colleagues (20). These results showed that cytosolic roGFP1 *in vivo* in CF15 cells (Fig. 2B) behaved very similarly to roGFP1 *in vitro* (20), though *in vivo* roGFP1 385/474 ratios were somewhat smaller than those exhibited *in vitro*.

We also tested if the genetic modification and differential subcellular localization of roGFP1 affected its fluorescence properties in nonpermeabilized cells. Intact CF15 cells expressing either cytosolic, mitochondrial, ER or surface roGFP1 were bathed in solutions containing different H_2O_2:DTT_{red} ([H_2O_2] + [DTT_{red}] = 10 mM), and roGFP1 ratios were measured in the different compartments. Since both H_2O_2 and DTT_{red} are membrane-permeant, these rapidly penetrated the intact cells and changed organelle roGFP1 ratios. These responses of each roGFP1 to solutions with different H_2O_2:DTT_{red} concentrations were compared by plotting directly measured roGFP1 ratios (Fig. 3A) and values that had been normalized such that maximal oxidized ratio values (obtained in 10 mM H_2O_2 solution) were set equal to 100% and maximal reduced ratio values (obtained in 10 mM DTT solution) were set equal to 0% for the four compartments (Fig. 3B).

As shown in Fig. 3A, absolute roGFP1 fluorescence ratios in the four compartments exhibited similar qualitative responses to the solutions containing different H_2O_2:DTT, but the magnitudes of the changes in roGFP1 fluorescence ratios from complete reduction (i.e., 0% oxidation, with 10 mM DTT) to complete oxidation (i.e., 100% oxidation, with 10 mM H_2O_2) were largest in the ER and smaller in the cytosol, mitochondria and at the cell surface. However, there were very similar responses of the normalized roGFP1 ratios in these compartments during incubation with the different H_2O_2:DTT_{red} solutions (Fig. 3B). These results validated the use of the probe for measuring redox potentials in different organelles, even though these all have different redox properties.

For subsequent experiments roGFP1 385/474 nm ratios recorded in the cytosol, mitochondria, ER and cell surface were converted to organelle redox potentials by treating intact cells at the end of each experiment with the membrane permeant DTT_{red} (10 mM) to attain maximal reduction and then with membrane permeant H_2O_2 (10 mM) to attain maximal oxidation. These maximal and minimal ratios were then used to generate

normalized roGFP1 ratios, which were then converted to redox potentials using the *in situ* calibration curve (Fig. 2B).

Redox properties of the cytosol, mitochondria, ER and cell surface in CF15 cells

Simultaneous analysis of the cytosolic, mitochondrial, ER, and cell surface redox properties was achieved by reseeding transfected cells (expressing cytosolic, mitochondrial, ER and cell surface roGFP1 in different cells) on one cover glass or by “co-transfection” with the four different plasmids (see Materials and Methods). A typical confocal image of three cells expressing cytosolic roGFP, three cells expressing mitochondrial roGFP, one cell expressing ER roGFP1 and two cells expressing surface roGFP1 obtained during excitation at 488 nm is shown in Fig. 4A. A single wavelength image obtained at the beginning of an experiment in the wide-field imaging microscope of a region containing multiple cells expressing the four compartment-specific roGFP1's is seen in Fig. 4B. The corresponding 385/474 ratio (pseudo color) image shows that roGFP1 expressed in the cytosol and mitochondria had low ratios characteristic of reduced roGFP1 (yellow-orange indicates reduced redox potentials) while ER and surface membrane had high ratios characteristic of oxidized roGFP1 (blue-green indicate oxidized redox potentials). Although the wide field imaging microscope and the resulting ratio images had lower resolution than the confocal images, it was easy to identify the ER-, mitochondria-, and cytosol-transfected cells: cytosolic roGFP1 was distributed evenly throughout the cytosol and nucleus, the surface probe was localized to the membrane and the ER- and mitochondria-roGFP's were localized to tubular or reticular structures throughout the cytosol but were excluded from the nucleus. Mitochondria and ER were distinguished by their very different roGFP1 ratios and also by the observation that mitochondria moved inside the cell, apparently along microtubules (38), while ER-roGFP1 remained static. The different redox potentials in the organelles can be visualized in the pseudo color image of Fig. 4C, which emphasizes the different ratios obtained in the cytosol, mitochondria, ER and outside surface of the plasma membrane in cells in the control condition at the beginning of the experiment.

Experiments were performed to test for redox regulation in the compartments by testing the effects of brief treatments with H_2O_2 and DTT. Representative responses of the cytosol, mitochondria, ER and membrane surface redox potentials of CF15 cells to oxidative and reductive challenge, all measured simultaneously in different cells, are shown in Fig. 4D. In untreated CF15 cells bathed in Ringer's solution, the roGFP1 ratio was most reduced (82%) in the cytosol, and consistently more oxidized in mitochondria (66%) (see Table 1). We detected no differences in roGFP1 ratio between the cytosol and nucleus. Converting these roGFP1 ratios to redox potentials showed cytosolic redox potential = -322 mV and mitochondrial redox potential = -344 mV (summarized in Table 1). Previous experiments on HeLa cells (21) yielded similar data showing that the cytosol (redox potential = -320 mV) was more oxidized than the mitochondria (redox potential = -360 mV).

roGFP1's expressed in the ER and at the cell surface of CF15 cells under control, untreated conditions were both much more oxidized (~ 5% reduced in both the ER and at the cell surface) than either the cytosol or mitochondria. It was difficult to calibrate these roGFP1 ratios in terms of precise redox potentials of the ER and cell surface under control conditions

because the roGFP1 ratios were nearly saturated, judged by the relatively small increase in roGFP1 385/474 ratio of the ER probe in response to 100 μM H_2O_2 indicating that ER and surface were more oxidized than about -250 mV. Upon washing the cells with fresh Ringers solution without H_2O_2, the cytosol and the mitochondria recovered from oxidation over a period of about one hour while there was little change in the roGFP1 ratio in ER and at the cell surface. Recovery of the redox potentials in the mitochondria and cytosol following transient H_2O_2-induced oxidation was indicative of the redox regulatory properties of these two organelles.

After adding 500 μM of the membrane permeable reductant dithiothreitol (DTT), the cytosol, mitochondria, ER and cell surface were reduced to -330 mV, -380 mV, -350 mV and -300 mV, respectively. Similar to the effects above, washing out the DTT lead to recovery of redox potentials to or towards control values observed at the beginning of the experiment, indicating that the cells had the capability of rapidly reoxidizing the cell surface, cytosol, mitochondria and ER. As further shown in Fig. 4D, the ER, cytosol and mitochondria recovered almost completely from reduction by a rapid reoxidation, with the rate of recovery in the ER larger than that in the cytosol and mitochondria. The cell surface exhibited only partial recovery after washing out the DTT. Further addition of 10 mM H_2O_2 caused the surface roGFP1 (as well as all the others) to oxidize to a redox potential higher than -250 mV as monitored at the beginning of the experiment (not shown), indicating that the probe was capable of responding to further oxidation but the cells were incapable of reoxidizing the surface probe on their own following this treatment with DTT. These data indicated that the mitochondria, ER, cytosol and cell surface all actively regulated their redox potentials. Mitochondria and cytosol of CF15 cells appeared to have the capability both to regulate their redox potentials to fairly precise, but different levels.

Although it was clear that the cell surface and, especially, the ER had mechanisms capable of rapid oxidation, the precise value of these oxidized redox potentials in the ER and the cell surface were difficult to determine. We therefore utilized an indirect method to determine these values. DTT was added in steps of increasing concentrations (10, 50, 100, 500 and 1000 μM) to CF15 cells expressing the various roGFP1 constructs, and 385/474 nm ratios were measured and calibrated. Results from one of these experiments are shown in Fig. 5A, where it can be seen that DTT had dose-dependent effects (threshold about 10 μM) to decrease the roGFP1 385/474 ratio in the ER and at the cell surface. A graph of the redox potentials in the ER and at the cell surface as a function of [DTT] is shown in Fig. 5B. Extrapolation of the ER plot to the y intercept, equivalent to [DTT] = 0, showed that the redox potential in the ER was -217 mV. Similar measurements for the cell surface showed that redox potential there was -207 mV (summarized in Table 1). Similar measurements were performed to test effects of increasing [H_2O_2] on redox potentials in the mitochondria and cytosol. The threshold response for both cytosol and mitochondria appeared to occur with 1 μM H_2O_2, and >100 μM was required to oxidize these compartments to levels exhibited by the ER.

Electrophysiological and redox properties of CF *vs* CFTR-corrected CF15 cells

We utilized adenovirus-CFTR to express wild-type CFTR in CF15 cells to test the role of CFTR in controlling redox potentials, buffering and regulation as performed in Fig. 4D. We first tested whether adenovirus-CFTR was inducing the key property of cyclic AMP-triggered Cl^- secretion across CF15 monolayers. We also tested for the presence of tight junctions, since these are required to generate transepithelial short circuit currents. Staining for the tight junction protein ZO-1 is shown in Fig. 6A and confirms epithelial differentiation of CF15 cells grown as monolayers on permeable filter inserts. CF15 cells grown on cover glasses were infected with an adenovirus coding for wild type CFTR-GFP chimera under control of a CMV promoter. After 24 hours fluorescence of CFTR-GFP was analyzed by confocal microscopy. Strong signals were detected in the cell periphery close to the apical pole and less but still significant expression at the basolateral membrane (Fig. 6B, upper panel). Intracellular CFTR expression was observed in the Golgi or recycling endosomes (larger accumulations of fluorescence in a perinuclear region). There was also weaker CFTR expression in the endoplasmic reticulum, most clearly evident in the nuclear membrane. There was no detectable CFTR-GFP expression in the mitochondria (see Fig. 1B for comparison). 3D reconstruction of XY scans in Fig. 6B (lower panel) showed CFTR-GFP expression in the apical membrane and only weak signal at the basal side. Apical CFTR localization suggested that cells grown to confluence on cover glasses differentiate with apical CFTR expression. Identical growth conditions were applied for ratiometric, fluorescence microscopy using roGFP1 to measure subcellular redox properties. Adenoviruses coding for ß-galactosidase (lacZ) and EGFP were used to control for viral infection and also to determine the number of cells infected by the adenovirus. As shown from ß-galactosidase activity (Fig. 6C) and EGFP fluorescence (Fig. 6D) of infected CF15 cells, 70-80% of CF15 cells were transduced using the adenoviral method. 10 other experiments showed that infection efficiencies varied between 70-100%.

Functional expression of CFTR in the apical membrane was tested by measuring cAMP-stimulated Cl^- secretion in CF15-lacZ and CF15-CFTR monolayers in the presence of the Na^+ channel blocker amiloride (20μM) (Fig. 7). This pharmacological regimen eliminates Na^+ absorption as a confounding current in evaluating effects on Cl^- secretion. Addition of forskolin (20 μM, to activate adenylate cyclase and increase cell [cAMP]) to the amiloride-treated monolayers increased I_{SC} in CF15-CFTR but not CF15-lacZ monolayers, and the forskolin-induced current was blocked by the chloride channel blocker diphenylamine-2-carboxylate (DPC, 5 mM apical) (Fig. 7A). These results were consistent with the idea that CFTR expression led to a forskolin-stimulated anion secretion. However, this effect did not reach significance under these experimental conditions (Fig. 7C). We therefore applied a serosal-to-mucosal Cl^- gradient to increase the electrochemical gradient for Cl^- secretion. Results from a typical experiment are shown in Fig. 7B. This treatment significantly and consistently increased the forskolin-stimulated I_{SC} (on average by a factor of seven) in eight out of eight experiments in CF15-CFTR but not CF15-lacZ monolayers (Figs 7B, C) and, again, DPC completely inhibited stimulated currents ($\Delta I_{sc,\ DPC} = -14.5 \pm 10.5\ \mu A/cm^2$, n=8). We also noted a L, but significant inhibitory effect of DPC in CF15-lacZ cells ($\Delta I_{sc,\ DPC} = -2.1 \pm 0.7\ \mu A/cm^2$, n=6, p=0.03 one-sample t-test), which might have been due to the inhibition of a residual ΔF508-CFTR activity or other non-CFTR Cl^- conductances in

these cells. However, these effects of DPC on baseline Cl^- currents in CF15-lacZ cells were small when compared to Cl^- currents of CF15-CFTR monolayers.

An experimental protocol similar to that shown in Fig. 4D was used to analyze the role of CFTR in affecting cellular redox properties. CF15 cells were first exposed either to Ad-CFTR or Ad-lacZ for 24 hrs. Then the cells were transfected with the four plasmids to generate roGFP1 expression in the cytosol, mitochondria, ER and membrane surface, and experiments were then performed after another 24-48 hrs. Steady state redox potentials were recorded at the beginning of each experiment, during addition of 100 μM H_2O_2, after recovery from this oxidative challenge (washing with Ringer's solution), then during addition of 500 μM DTT and finally after recovery from reductive challenge (washing with Ringer's solution). If there were CFTR-dependent differences in redox regulation in the ER, mitochondria, cytosol or cell surface (e.g., different [GSH]:[GSSG] or different rates of ROS production), one would expect that CF15-CFTR cells would differ from CF15-lacZ cells in their redox states and/or regulatory properties.

The initial redox potentials for each compartment recorded at the beginning of experiments are seen in Table 1. During control conditions the mitochondria (-345 mV) were more reduced than the cytosol (avg = - 320 mV), and there was no statistical difference between CF15-lacZ and CF15-CFTR. roGFP1 expressed at the extracellular surface of the plasma membrane and also in the ER was nearly completely oxidized since the sensor responded to H_2O_2 with only small or no changes in 385/474 nm ratio. These did not appear to be different in CF and CFTR-corrected cells (Table 1), but difficulty in accurate calibrations of the ER and surface under control conditions precluded an accurate measurement.

Further information about redox properties of the organelles was obtained by testing redox regulatory properties: magnitudes and rates of changes of redox potentials in the subcompartments were monitored following addition and then removal of either DTT or H_2O_2 to the bathing solutions, similar to the protocol shown in Fig. 4D. 100 μM H_2O_2 oxidized the cytosol and mitochondria by similar amounts (Fig. 8A) and at similar rates (Fig. 9A) in CF15-lacZ and CF15-CFTR cells. Similarly, following washout of the H_2O_2 from the solution, mitochondria and cytosol recovered nearly completely to the control levels and at similar rates in CF15-lacZ and CF15-CFTR cells (Figs. 8A and 9A). Treatment of both CF and CFTR-corrected cells with 500 μM DTT elicited reduction of both the ER and the cell surface, and the magnitudes (Fig. 8B) and time courses (Fig. 9B) of these responses were similar in the CF15-lacZ and CF15-CFTR cells. Following washout of the DTT, CF and CFTR-corrected cells only partially reoxidized the extracellular face of the plasma membrane, while the ER lumen reoxidized rapidly and completely. There were no significant differences in the magnitudes (Fig. 8B) or time courses (Fig. 9B) of these responses between CF15-lacZ and CF15-CFTR cells. The effect of 10 μM forskolin to stimulate CFTR by increasing cytosolic cAMP was tested on the four subcellular locations but did not affect any redox properties (not shown). We also found no differences in the redox properties of organelles of non-infected CF15 compared to lacZ-infected CF15 cells, suggesting that the adenoviral infection did not affect the redox properties in these cells.

Although there were no differences between CF and CFTR-corrected cells, responses of the organelles to H_2O_2 and DTT indicated selective responses. Thus, DTT caused larger and faster reduction of the ER than the cell surface, and reoxidation was also larger and faster in the ER than at the cell surface (Figs. 8B and 9B). In contrast, H_2O_2 application and removal appeared to elicit similar rates and magnitudes of changes in redox potentials in the mitochondria and cytosol (Figs. 8A and 9A).

Oxidation of the apical solution measured with Amplex Red and of the cell interior measured with carboxy-dichlorodihydrofluoresceindiacetate

For comparison we investigated the effects of CFTR expression on redox state using two additional approaches to verify the results obtained with targeted roGFP1. We utilized the Amplex Red method to measure rates of oxidation of the apical solution bathing CF15 cells and carboxy-H_2DCFDA to assay rates of oxidation of this probe in the cytosol in CF and CFTR-corrected cells. Amplex Red and HRP were added to the apical solution of CF15 cells grown on filters, and rates of increase of fluorescence were measured and converted to rates of H_2O_2 production (see Methods). Results from a typical experiment showing the generation of apical H_2O_2 by differentiated CF15-lacZ and CF15-CFTR cells grown on permeable supports is shown in Fig. 10A. There was no increase in Amplex Red fluorescence with time in the absence of cells, showing that the cells were the source of the H_2O_2 measured using this method. Both CF and CFTR-corrected cells continuously released H_2O_2 into the apical solution at similar rates, 464 pmole·cm^{-2}·h^{-1} in CF15-lacZ and 445 pmole·cm^{-2}·h^{-1} in CF15-CFTR. These data were consistent with the surface roGFP1 measurements showing that CF15-lacZ and CF15-CFTR cells had the same redox potentials in control conditions and reoxidized the surface following reduction at similar rates.

Oxidation of the nonfluorescent, membrane permeant dye carboxy-H_2DCFDA to the oxidized, membrane impermeant dye DCF by the cells was used as a second test of the oxidative properties of CF and CFTR-corrected cells. Cells grown on permeable supports were exposed to 5 μM carboxy-H_2DCFDA on the apical surface, and fluorescence inside the cells was measured. As shown in Fig. 10B, CF15-lacZ and CF15-CFTR cells oxidized the H_2DCFDA at equal rates, indicating that CFTR expression did not alter the bulk oxidative capabilities of the cells.

Small thiol molecules as redox state reporters in CF *vs* CFTR-corrected CF15 cells

To gain further information about redox properties of CF and CFTR-corrected CF15 cells and also to confirm data obtained using fluorescent redox sensors, we analyzed GSH, GSSG, cysteine and cystine levels by HPLC and adjusted concentrations to account for dilution during processing and cell volume. We first tested whether the expression of roGFP1 might influence measurements. If expression of roGFP1 itself altered the cellular redox state, one would expect changes in the concentration and the ratio of the GSH:GSSG- or cysteine:cystine redox couple. We therefore compared small molecule levels in roGFP1-transfected CF15 cells with non-transfected cells. As seen in Figs 11A and B, expression of roGFP1 did not significantly changed cellular levels of GSH (8.2 ±0.4 mM), GSSG (101 μM ± 8 μM), cysteine (138 μM ± 17 μM) or cystine (22 μM ± 5 μM).

If CFTR affected redox properties other than those analyzed with either roGFP1, carboxy-H_2DCFDA or Amplex Red, differences might be detected from changes in the concentrations of small, redox-active molecules. We compared GSH, GSSG, cysteine and cystine levels in cell lysates of CF15-lacZ and CF15-CFTR cells. The composition of these small molecules in the apical fluid was assayed by culturing CF- and CFTR- corrected cells on permeable support to allow complete polarization and analysis of the apically secreted fluid.

GSH and GSSG concentrations are shown in Fig. 11A. There were no significant differences between CF and CFTR-corrected cells in either cell lysates or apical fluids: $GSH:GSSG_{(cellular)}$: 8.7 mM : 0.1 mM in CF15-lacZ vs. 8.8 mM : 0.1 mM in CF15-CFTR cells; $GSH:GSSG_{(apical\ fluid)}$: 565 μM: 38 μM in CF15-lacZ vs. 568 μM : 71 μM in CF15-CFTR cells. Cysteine levels were upregulated upon adenoviral infection, though calculated redox potentials were only slightly affected by the virus. CF15-lacZ- and CF15-CFTR cells showed no significant differences in cysteine or cystine concentration detected in cell lysates (209 μM ± 13 μM vs. 203 μM ± 36 μM) and apical secretions (Fig. 11B). Interestingly, cysteine and cystine levels were higher in the apical fluid of CF15-lacZ and CF15-CFTR cells (353 μM ± 19 μM vs. 345 μM ± 11 μM) compared to intracellular concentrations.

Redox potentials for each redox couple were calculated from their concentrations using the Nernst equation (see Table 2). Results from these experiments indicated very similar intracellular regulation of the GSH:GSSG couple (about -260 mV) for both CF15-lacZ and CF15-CFTR cells. There was similar apparent regulation of the cysteine:cystine couple (-160 mV to -170 mV) in CF15 and roGFP1-expressing CF15 cells and in CF15-lacZ and CF15-CFTR cells. Calculated redox potentials of the apical fluid of CF15-lacZ and CF15-CFTR cells were also very similar for both the glutathione redox couple (-194 to -202 mV) and also for the cysteine redox couple (-153 to -154 mV). These data suggest that CFTR expression did not significantly affect any of these redox couples in CF15 cells or in the apical surface liquid, though adenoviral infection increased cellular concentration of cysteine and slightly decreased the redox potential of the cysteine:cystine couple.

Discussion

Genetic targeting of roGFP1 to the cell surface, cytosol, mitochondria and ER, and a novel transfection protocol allowed simultaneous measurements of redox potentials in all these compartments. The reversible, ratiometric output of roGFP1 was useful compared to biochemical measurements of oxidized:reduced ratios of glutathione ([GSSG]:[GSH]) because this method destroys the cells, preventing long-term observations. This approach also does not include potential contributions of other redox regulators to the redox potentials. roGFP1 is also preferable to using electron spin resonance because this method requires adding high concentrations of spin traps (39,40) to dissociated cells in cuvettes; ESR methods are also not useful for measurements in organelles in intact cells. Carboxy-H_2DCFDA has been used here and by others to measure oxidation of the cytosol and Amplex Red to measure oxidation of the cell surface, but these methods are disadvantageous because they measure only accumulation of oxidized, fluorescent products and therefore do not permit measurements of reversible oxidation-reduction processes in different

compartments. In addition, genetic targeting permitted measurements of specific compartments compared to the fluorescent dyes, which measure the sum total of the activities of different cellular compartments. For example, it is often assumed that adding carboxy-H_2DCFDA to cells (as in Fig. 10B) leads to oxidation of the dye in the cytosol and therefore yields information about redox processes in this compartment. However, results obtained with roGFP1 show that the cytosol, mitochondria and ER are all capable of performing oxidation reactions, so it seems possible that all these compartments may contribute to oxidative production of DCF in intact cells. Genetic targeting combined with the sequential transfection method should also prove useful for experiments in which knowledge about the time course of changes in different compartments is important.

Although roGFP1 can be accurately calibrated *in vitro* (20,21), quantitative calibration of roGFP1 *in vivo* has proven to be somewhat difficult. To calibrate roGFP1 fluorescence ratios *in vivo* we first incubated cells that had been permeabilized with digitonin to allow permeation of DTT_{red}:DTT_{ox} redox buffers, all in deoxygenated solutions. By applying partial permeabilization in combination with ≥ 10 mM DTT standard solutions we tried to keep the cellular environment intact while also assuring equilibrium between the cytosol and bath solution. The resulting *in situ* calibration curve had a slope and midpotential (-276 mV) similar to the slope and midpotential (-288 mV) of the *in vitro* calibration curve obtained with isolated, recombinant roGFP1 (20). The different midpotentials measured *in situ* (Fig. 2B) and *in vitro* (20) may result from different environments of roGFP1 *in vitro* and *in situ* (e.g., isolation condition for recombinant roGFP1, different buffer composition, interacting enzymes), but it is also possible that subtle differences in calibration methods contributed to the differences. For example, our calibrations, but not those of Hanson and colleagues (20), included treating cells with both 10 mM DTT and 10 mM H_2O_2 to obtain maximal reduction and oxidation of roGFP1, thereby allowing comparison among experiments. Thus, even though roGFP1 is nearly entirely oxidized when exposed to DTT_{ox}: DT_{Tred} standard solutions with a calculated redox potentials of -222 mV, further addition of 10 mM H_2O_2 still had a slight oxidizing effect on the roGFP1 ratio (Fig. 2A). Titrations with DTT:H_2O_2 mixtures showed that even though roGFP1 ratios increased with oxidation to a greater extent in the ER than in the cytosol, mitochondria, and cell surface (Fig. 3A), normalized organelle roGFP1 ratios responded very similarly in all the compartments (Fig. 3B). Overall, these data showed that roGFP1 behaved similarly in all the organelles and indicated that the probe was useful for performing experiments in all these compartments in intact CF15 cells.

The present data showed that cytosolic redox potentials in CF15 cells averaged -322 mV, very similar to previous roGFP1 measurements of cytosolic redox in both HeLa (-320 mV, see Table 1 and 21) and *Arabidopsis* cells (-320 mV; 41). Measurements in yeast with a redox-sensitive YFP (42) showed that the cytosolic redox potential (-289 mV) was 30 mV (Table 1 and 21) more oxidized than values measured in mammalian and plant cells using roGFP1. Whether this difference can be attributed to different methods, probe or cell type remains to be determined. CF15 mitochondria (-345 mV, Table 1) were more oxidized than those in HeLa cells (-370 mV, 20,21) and *Arabidopsis* (-360 mV, 41). All the GFP-based measurements of cytosolic and mitochondrial redox potentials were more reduced than predicted from measurements of bulk cellular GSH/GSSG ratios (Table 2; 43, 44). The

present results further showed that mitochondria and cytosol exhibited similar oxidations in response to increases in [H_2O_2]. However, at concentrations above 50 μM, both cytosol and especially mitochondria were quite resistant to the effects of H_2O_2. Both cytosol and mitochondria recovered from both oxidation (H_2O_2) and reduction (DTT) at similar rates. Thus, even though regulatory mechanisms may differ in mitochondria and cytosol, both mitochondria and cytosol were relatively resistant to effects of H_2O_2 over the range of 10-100 μM, and redox regulation following brief treatments with either H_2O_2 or DTT occurred with similar kinetics in the two compartments.

The ER and cell surface were both more oxidized than cytosol and mitochondria, as indicated by nearly totally oxidized roGFP1. Although precise calibrations of the ER and cell surface of control cells were difficult, extrapolation of the redox potentials in the ER or at the cell surface vs. [DTT_{red}] to zero gave an estimate of the ER redox potential of -217 ± 1mV and surface redox potential of -207 ± 8 mV. Previous estimates of ER redox potentials from measurements of total glutathione concentrations and [GSH]:[GSSG] ratios and calculations using the Nernst equation have yielded estimates of -133 to -185 mV (43,27). There have been no previous estimates of redox potential at cell surfaces. Both ER and cell surface were capable of re-oxidation following brief reduction with DTT, though the cell surface exhibited only incomplete re-oxidation compared to that the ER. The mechanisms leading to these oxidations are unknown. Protein disulfide isomerase (PDI) in the ER contributes importantly to S-S bond formation (19), and PDI has also been found at the external surface of the plasma membrane (44), so PDI may contribute to the re-oxidation in both locations. The roles of other enzymes (e.g., Ero1 and Erv2) and cofactors (e.g., FAD) that also participate in protein oxidation in the ER (19) remain to be determined. Airway epithelial cells express NADPH oxidase (Nox)-like protein Duox1 on their apical membranes (9), and oxidation of the apical solution measured with Amplex Red is partially blocked by the Nox blocker diphenyleneiodonium (DPI, 5 μM), so Duox1 is a potential mechanism to oxidize the surface membrane as measured with roGFP1 (Fig. 4D) and the apical solution as measured with Amplex Red (Fig. 10A). Results from the Amplex Red experiments indicate constant efflux of H_2O_2 by CF15 cells over time without changes in the rate of oxidation, while roGFP1 at the cell surface was reoxidized upon DTT removal to some degree and reached a plateau at about -270 mV. This apparent contradiction may be explained as follows. This oxidation of surface-roGFP1 depends on oxidative equivalents but equilibrates with its environment (e.g., antioxidants like GSH or other cell surface proteins). In contrast, oxidation of Amplex Red depends on the generation of H_2O_2 by the cell since the substrate (Amplex Red) and horse radish peroxidase are not limiting factors in the system. A plateau of the Amplex Red oxidation would be expected to be seen only if all the substrate were converted to its fluorescent conformation.

In addition to its Cl^- channel function, CFTR has been proposed to conduct GSH (8,1,45) and also to downregulate adjacent ENaC activity (11, 46,12,) such that in CF upregulated Na^+ transport (47,48,49) leads to increased O_2 consumption (14) and cellular hypoxia (10). Hypoxia like that observed for CF airway epithelial cell cultures is known to increase mitochondrial production of ROS (50, 15,16,51), and recent measurements of mitochondrial GSH and DNA oxidation have given indications that CF mitochondria are oxidized compared to nonCF (17). However, experiments using roGFP1 here showed that adenoviral

expression of CFTR did not alter redox regulatory properties of the cell surface, mitochondria, cytosol or ER. Based on lacZ and EGFP expression the adenovirus infected a large majority (70-100%) of cells. The fact that lacZ-transduced CF15 cells behaved similarly to the untreated cells, with the exception that cysteine and cystine levels were increased by about a third, indicated that the adenovirus itself had little effect on either the ion transport or redox regulation of the cells.

Functional expression of CFTR after AdCFTR infection of confluent CF15 monolayers was verified in Ussing chambers. CFTR expression in CF15 cells caused an increase in forskolin-stimulated I_{SC}, i.e., anion (likely either Cl or HCO_3^-) secretion that was small (2 $\mu A/cm^2$) when the cells were incubated with equal concentrations of Cl^- on each side of the monolayer, consistent with results obtained with other CFTR-expressing cell culture models like nonciliated human tracheal cultures (52) and Calu-3 cells (24,30). Currents were larger (approx. 15 $\mu A/cm^2$) in the presence of a serosa-to-mucosa gradient of Cl^-. In both circumstances, the forskolin-stimulated I_{SC} was blocked by mucosal DPC, a CFTR and Cl^- channel blocker (53). This is consistent with the idea that the cell-apical solution electrochemical gradient for Cl^- was small when both solutions contained normal [Cl^-], so forskolin treatment caused only a small increase in current even though the CFTR opened. Currents were larger when the apical solution contained no Cl^- because the cell-to-apical electrochemical gradient for Cl^- was increased so that Cl^- left the cell through the activated CFTR. The need for a Cl^- gradient as a driving force both to secrete Cl^- across the apical membrane and to increase the sensitivity of the assay has been recognized previously (24,54,55,56).

In contrast to the effects of CFTR expression to increase Cl transport, there were no differences in either steady state redox properties or regulation between CF and CFTR-corrected cells using any of the tested assays. Steady state redox potentials measured using roGFP1 were the same for the cell surface, cytosol, mitochondria and ER for CF15-lacZ and CF15-CFTR cells. In addition, rates of oxidation of the cells (as measured with carboxy-H_2DCFDA) or the surface fluid (as measured with Amplex Red) were similarly unaffected by CFTR expression. These data were consistent with measurements of cysteine:cystine and GSH:GSSG, which also showed no differences between CF15-lacZ and CF15-CFTR cells in steady state concentrations of cell extracts or surface liquid. Although there were unexplained increases in cysteine and cystine concentrations in cell lysates of CF15-lacZ- and CF15-CFTR cells, the changes were identical for both CFTR-and lacZ-expressing cells, consistent with the GSH:GSSG and roGFP1 measurements showing no redox differences between CF and CFTR-corrected cells. In addition, rates of redox regulation (as measured with roGFP1) for the cytosol, mitochondria, ER and cell surface were unaffected by CFTR expression. Stimulation of CFTR by forskolin also had no effect on the redox state as measured with roGFP1.

It has been reported (6, 57) that there are different GSH concentrations in CF (78 μM) vs. non-CF (257 μM) BAL fluid, while GSSG concentrations were approximately the same (14 v. 21 μM), indicating a more oxidized environment in the BAL fluid in CF patients. These data were consistent with results obtained on CFTR knock out mice vs. non-CF mice (7). In contrast, our experiments showed that CF15 cells secreted similar amounts of GSH (565-568

μM) and GSSG (38-71 μM) into the surface liquid as observed in BAL fluid *in vivo* (6, 57), but there were no differences in our GSH:GSSG (or cysteine:cystine) ratios between CF and CFTR-corrected cells. Our results obtained for total GSH from cell lysates (8.7 mM vs. 8.8 mM in CF vs non-CF, respectively) were consistent with data obtained both *in vitro* (1) and *in vivo* (7) showing no difference in cellular or tissue concentrations of GSH in CF vs. non-CF cells. Our experiments also showed that there was a large gradient between intracellular GSH (8.8 mM) and apical fluid (568 μM). These data suggested that, even though CFTR has the capacity to transport GSH and therefore might be expected to affect both cytosolic and surface liquid redox properties, transporters other than CFTR might control GSH transport (58) so that there were no differences between CF and CFTR-corrected cells. Differences between our results obtained *in vitro* and previous data *in vivo* (6, 57) and *in vitro* (1) may have arisen from such problems as contaminating neutrophils, bacteria or bacterial products *in vivo* and from difficulties in cell matching *in vitro*. We avoided these problems by working *in vitro* using one cell type and the adenoviral approach to assure isogenic comparisons.

Mitochondrial GSH levels have also been reported to be lower in both lung cells from CFTR knock out mice and nonCF mice and also in cultured human CF (IB3) vs. CFTR-corrected (C38) cells (59). In contrast, the present data showed no differences in mitochondrial redox potentials between CF and CFTR-corrected cells. It is possible that differences in mitochondrial redox potentials between CF15 and CFTR-corrected CF15 cells were too small to measure with our method – assuming mitochondrial [GSH] = 10 mM in non-CF or CFTR-corrected cells and using data in Fig. 2 from Day et al (59) and the Nernst equation, we calculate that mitochondrial redox potentials would have been more oxidized by only 6-8 mV in IB3 (CF) compared to C38 (CFTR-corrected) cells. Alternatively, it is also possible that the CF15 cells have different mitochondrial GSH transport mechanisms compared to the IB3-C38 cells. For example, since cellular GSH and GSSG concentrations (and ratios and calculated or measured redox potentials) do not appear to be markedly different in CF vs CFTR-corrected cells (present data and 1, 7, 57), differences in mitochondrial redox could have arisen from altered mitochondrial GSH resulting from some CFTR-dependent uptake mechanism in the mitochondrial membrane (59).

Although the data showed there were no differences in the redox properties of CF vs. CFTR-corrected cells, there were differences in the values measured using the different methods. Redox potentials calculated from biochemical assays of cell lysates were ~-170 mV for the cysteine redox couple and ~-260 mV for the glutathione redox couple, while cytosolic redox potentials measured with roGFP1 were substantially more reduced (~-320 mV). One explanation for this difference is that the more positive potentials calculated from small molecule redox couples isolated from cell lysates may be contaminated by contributions from the highly oxidized compartments. This hypothesis is supported by analysis of redox potentials in the apical fluid which was collected without cell lysis: similar redox potentials were calculated from GSH:GSSG (~-200 mV) and measured with roGFP1 (-207 mV). Potentials calculated from the cysteine:cystine couple were more oxidized (~-150 mV) and therefore not in equilibrium with the GSH:GSSG couple. Jones *et al.* (60) suggest that GSH:GSSG, cysteine:cystine and also thioredoxins represent redox systems which are

individually regulated. It therefore seems possible that the redox couples might be affected by each other but also respond differently to redox-modifying enzymes. In addition, roGFP1 might be affected by the thioredoxin system (61), which would explain the more reduced potentials measured with roGFP1 in the cytosol and mitochondria, based on the presence of thioredoxin 1 in the cytosol and thioredoxin 2 in the mitochondria (which both have E^0 of about ~-280 mV (60,62)). The conformation of roGFP1 found in the ER (-217 mV) and at the cell surface (-207 mV) is likely to be under the control of luminal or cell membrane-bound PDI, which is also a member of the thioredoxin superfamily and has an equilibrium potential around -160 mV (62).

In summary, this paper provides the first comprehensive analysis of how CFTR affects redox environments both within and outside of lung epithelial cells. The inclusion of both real time measurements of redox potentials using roGFP1 in multiple compartments in combination with other probes and measurements of small molecule thiol redox states provided a detailed coverage to detect any subtle changes in redox environment potentially controlled by CFTR. The fact that all the probes did not measure the same redox potentials and thus were likely to be in disequilibrium suggested that our multiple approaches provided good coverage from -320 mV (close to E^0 for thioredoxin and NADPH) to -260 mV/-220 mV (GSH) and -180 mV/-100 mV (cysteine). The highly sensitive redox probes carboxy-H_2DCFDA and Amplex Red also failed to detect a role for CFTR in altering redox. Thus, CFTR increased Cl^- secretion without altering redox properties of the cytosol, cell surface, mitochondria or ER in CF15 airway epithelia cells.

Acknowledgments

Roger Tsien and Colette Dooley provided critical advice and suggestions. Supported by grants from the NIH [DK51799 (TEM), GM043618-14 (SJR), HL071829 (HF)], Cystic Fibrosis Foundation [CFFMACH03 (TEM) and CFFSCHWAR04F0 (CS)] and Cystic Fibrosis Research Inc.

References

1. Gao L, Kim KJ, Yankaskas JB, Forman HJ. Abnormal glutathione transport in cystic fibrosis airway epithelia. Am. J. Physiol. Lung Cell. Mol. Physiol. 1999; 277:L113–L118.
2. Hartl D, Starosta V, Maier K, Beck-Speier I, Rebhan C, Becker BF, Latzin P, Fischer R, Ratjen F, Huber RM, Rietschel E, Krauss-Etschmann S, Griese M. Inhaled glutathione decreases PGE(2) and increases lymphocytes in cystic fibrosis lungs. Free Radic. Biol. Med. 2005; 39:463–472. [PubMed: 16043018]
3. Bishop C, Hudson VM, Hilton SC, Wilde C. A pilot study of the effect of inhaled buffered reduced glutathione on the clinical status of patients with cystic fibrosis. Chest. 2005; 127:308–317. [PubMed: 15653998]
4. Hudson VM. New insights into the pathogenesis of cystic fibrosis: pivotal role of glutathione system dysfunction and implications for therapy. Treat. Respir. Med. 2004; 3:353–363. [PubMed: 15658882]
5. Kabe Y, Ando K, Hirao S, Yoshida M, Handa H. Redox regulation of NF-kappaB activation: distinct redox regulation between the cytoplasm and the nucleus. Antioxid. Redox Signal. 2005; 7:395–403. [PubMed: 15706086]
6. Roum JH, Buhl R, McElvaney NG, Borok Z, Crystal RG. Systemic deficiency of glutathione in cystic fibrosis. J. Appl. Physiol. 1993; 75:2419–2424. [PubMed: 8125859]

7. Velsor LW, van Heeckeren A, Day BJ. Antioxidant imbalance in the lungs of cystic fibrosis transmembrane conductance regulator protein mutant mice. Am. J. Physiol. Lung Cell Mol. Physiol. 2001; 281:L31–38. [PubMed: 11404242]
8. Linsdell P, Hanrahan JW. Glutathione permeability of CFTR. Am. J. Physiol. Cell Physiol. 1998; 275:C323–C326.
9. Schwarzer C, Machen TE, Illek B, Fischer H. NADPH oxidase-dependent acid production in airway epithelial cells. J. Biol. Chem. 2004; 279:36454–36461. [PubMed: 15210697]
10. Worlitzsch D, Tarran R, Ulrich M, Schwab U, Cekici A, Meyer KC, Birrer P, Bellon G, Berger J, Weiss T, Botzenhart K, Yankaskas JR, Randell S, Boucher RC, Doring G. Effects of reduced mucus oxygen concentration in airway Pseudomonas infections of cystic fibrosis patients. J. Clin. Invest. 2002; 109:317–325. [PubMed: 11827991]
11. Stutts MJ, Canessa CM, Olsen JC, Hamrick M, Cohn JA, Rossier BC, Boucher RC. CFTR as a cAMP-dependent regulator of sodium channels. Science. 1995; 269:847–850. [PubMed: 7543698]
12. Stutts MJ, Rossier BC, Boucher RC. Cystic fibrosis transmembrane conductance regulator inverts protein kinase A-mediated regulation of epithelial channel single channel kinetics. J. Biol. Chem. 1997; 272:14037–14040. [PubMed: 9162024]
13. Peckham D, Holland E, Range S, Knox AJ. Na+/K+ ATPase in lower airway epithelium from cystic fibrosis and non-cystic-fibrosis lung. Biochem. Biophys. Re.s Commun. 1997; 232:464–468.
14. Stutts MJ, Knowles MR, Gatzy JT, Boucher RC. Oxygen consumption and ouabain binding sites in cystic fibrosis nasal epithelium. Pediatr. Res. 1986; 20:1316–1320. [PubMed: 2432456]
15. Chandel NS, Maltepe E, Goldwasser E, Mathieu CE, Simon MC, Schumacker PT. Mitochondrial reactive oxygen species trigger hypoxia-induced transcription. Proc. Natl. Acad. Sci. 1998; 95:11715–11720. [PubMed: 9751731]
16. Chandel NS, McClintock DS, Feliciano CE, Wood TM, Melendez JA, Rodriguez AM, Schumacker PT. Reactive oxygen species generated at mitochondrial complex III stabilize hypoxia-inducible factor-1 during hypoxia: A mechanism of O2 sensing. J. Biol. Chem. 2000; 275:25130–25138. [PubMed: 10833514]
17. Velsor LW, Kariya C, Kachadourian R, Day BJ. Mitochondrial Oxidative Stress in the Lungs of Cystic Fibrosis Transmembrane Conductance Regulator Protein Mutant Mice. Am. J. Respir. Cell Mol. Biol. Jun 8.2006 [Epub ahead of print].
18. Weber AJ, Soong G, Bryan R, Saba S, Prince A. Activation of NF-kappaB in airway epithelial cells is dependent on CFTR trafficking and Cl-channel function. Am. J. Physiol. Lung Cell Mol. Physiol. 2001; 281:L71–78. [PubMed: 11404248]
19. Sevier CS, Kaiser. C.A. Formation and transfer of disulphide bonds in living cells. Nature Rev. Mol. Cell. Biol. 2002; 3:836–847. [PubMed: 12415301]
20. Hanson GT, Aggeler R, Oglesbee D, Cannon M, Capaldi RA, Tsien RY, Remington SJ. Investigating mitochondrial redox potential with redox-sensitive green fluorescent protein indicators. J. Biol. Chem. 2004; 279:13044–13053. [PubMed: 14722062]
21. Dooley CT, Dore TM, Hanson G,T, Jackson WC, Remington SJ, Tsien RY. Imaging dynamic redox changes in mammalian cells with green fluorescent protein indicators. J. Biol. Chem. 2004; 279:22284–22293. [PubMed: 14985369]
22. Jefferson DM, Valentich JD, Marini FC, Grubman SA, Iannuzzi MC, Dorkin HL, Li M, Klinger KW, Welsh MJ. Expression of normal and cystic fibrosis phenotypes by continuous airway epithelial cell lines. Am. J. Physiol. 1990; 259:L496–505. [PubMed: 1701980]
23. Pizurki L, Morris MA, Chanson M, Solomon M, Pavirani A, Bouchardy I, Suter S. Cystic fibrosis transmembrane conductance regulator does not affect neutrophil migration across cystic fibrosis airway epithelial monolayers. Am. J. Pathol. 2000; 156:1407–1416. [PubMed: 10751364]
24. Illek B, Yankaskas J, Machen TE. cAMP- and genistein-stimulated HCO_3 secretion through CFTR in human airway epithelia. Am. J. Physiol. 1997; 272:L752–L761. [PubMed: 9142951]
25. Hybiske K, Ichikawa J, Huang V, Lory SJ, Machen TE. Cystic fibrosis airway epithelial cell polarity and bacterial flagellin determine host response to P. aeruginosa. Cell. Micro. 2004; 6:49–62.

26. Van Itallie CM, Anderson JM. The molecular physiology of tight junction pores. Physiology. 2004; 19:331–338. [PubMed: 15546850]
27. Schafer FQ, Buettner GR. Redox environment of the cell as viewed through the redox state of the glutathione disulfide/glutathione couple. Free Radic. Biol. Med. 2001; 30:1191–1212. [PubMed: 11368918]
28. Chandy G, Grabe M, Moore HP, Machen TE. Proton leak and CFTR in regulation of Golgi pH in respiratory epithelial cells. Am. J. Physiol. Cell. Physiol. 2001; 281:C908–21. [PubMed: 11502568]
29. Wunderlich, E. PhD thesis. University of California at Berkeley; 2003.
30. Wu MM, Grabe M, Adams S, Tsien RY, Moore HP, Machen TE. Mechanisms of pH regulation in the regulated secretory pathway. J. Biol Chem. 2001; 276:33027–33035. [PubMed: 11402049]
31. Wu MM, Llopis J, Adams S, McCaffery JM, Kulomaa MS, Machen TE, Moore HP, Tsien RY. Organelle pH studies using targeted avidin and fluorescein-biotin. Chem. Biol. 2000; 7:197–209. [PubMed: 10712929]
32. Kim JH, Johannes L, Goud B, Antony C, Lingwood CA, Daneman R, Grinstein S. Noninvasive measurement of the pH of the endoplasmic reticulum at rest and during calcium release. Proc. Natl. Acad. Sci. U S A. 1998; 95:2997–3002. [PubMed: 9501204]
33. Paroutis P, Touret N, Grinstein S. The pH of the secretory pathway: measurement, determinants, and regulation. Physiology. 2004; 19:207–215. [PubMed: 15304635]
34. Husek P, Matucha P, Vránková A, Simek P. Simple plasma work-up for a fast chromatographic analysis of homocysteine, cysteine, methionine and aromatic amino acids. J. Chromatogr. B. Analyt. Technol. Biomed. Life Sci. 2003; 789:311–22.
35. Boudreault F, Grygorczyk R. Cell swelling-induced ATP release is tightly dependent on intracellular calcium elevations. J. Physiol. 2004; 561:499–513. [PubMed: 15579539]
36. Tarran R, Button B, Boucher RC. Regulation of normal and cystic fibrosis airway surface liquid volume by phasic shear stress. Annu Rev Physiol. 2006; 68:543–61. [PubMed: 16460283]
37. Illek B, Fischer H. Flavonoids stimulate Cl conductance of human airway epithelium in vitro and in vivo. Am. J. Physiol. 1998; 275:L902–910. [PubMed: 9815107]
38. Hollenbeck PJ, Saxton WM. The axonal transport of mitochondria. J. Cell Sci. 2005; 118:5411–549. [PubMed: 16306220]
39. Sanlioglu S, Engelhardt JF. Cellular redox state alters recombinant adeno-associated virus transduction through tyrosine phosphatase pathways. Gene Ther. 1999; 6:1427–1437. [PubMed: 10467367]
40. Sanlioglu S, Williams CM, Samavati L, Butler NS, Wang G, McCray PB Jr. Ritchie TC, Hunninghake GW, Zandi E, Engelhardt JF. Lipopolysaccharide induces Rac1-dependent reactive oxygen species formation and coordinates tumor necrosis factor-alpha secretion through IKK regulation of NF-kappa B. J. Biol. Chem. 2001; 276:30188–30198. [PubMed: 11402028]
41. Jiang K, Schwarzer C, Lally E, Zhang S, Ruzin S, Machen T, Remington SJ, Feldman L. Expression and characterization of a redox-sensing green fluorescent protein(reduction-oxidation-sensitive green fluorescent protein) in Arabidopsis. Plant Physiol. 2006; 141:397–403. [PubMed: 16760494]
42. Ostergaard H, Tachibana C, Winther JR. Monitoring disulfide bond formation in the eukaryotic cytosol. J. Cell. Biol. 2004; 166:337–345. [PubMed: 15277542]
43. Hwang C, Sinskey AJ, Lodish HF. Oxidized redox state of glutathione in the endoplasmic reticulum. Science. 1992; 257:1496–1502. [PubMed: 1523409]
44. Janiszewski M, Lopes LR, Carmo AO, Pedro MA, Brandes RP, Santos CX, Laurindo FR. Regulation of NAD(P)H oxidase by associated protein disulfide isomerase in vascular smooth muscle cells. J. Biol. Chem. 2005; 280:40813–40819. [PubMed: 16150729]
45. Kogan I, Ramjeesingh M, Li C, Kidd JF, Wang YC, Leslie EM, Cole SPC, Bear CE. CFTR directly mediates nucleotide-regulated glutathione flux. EMBO J. 2003; 22:1981–1989. [PubMed: 12727866]
46. Mall M, Hipper A, Greger R, Kunzelmann K. Wild type but not deltaF508 CFTR inhibits Na+ conductance when coexpressed in Xenopus oocytes. FEBS Lett. 1996; 381:47–52. [PubMed: 8641437]

47. Boucher RC, Stutts MJ, Knowles MR, Cantley L, Gatzy JT. Na+ transport in cystic fibrosis respiratory epithelia. Abnormal basal rate and response to adenylate cyclase activation. J. Clin. Invest. 1986; 78:1245–1252. [PubMed: 3771796]
48. Boucher RC, Cotton CU, Gatzy JT, Knowles MR, Yankaskas JR. Evidence for reduced Cl- and increased Na+ permeability in cystic fibrosis human primary cell cultures. J. Physiol. 1988; 405:77–103. [PubMed: 3255805]
49. Willumsen NJ, Boucher RC. Shunt resistance and ion permeabilities in normal and cystic fibrosis airway epithelia. Am. J. Physiol. 1989; 256:C1054–1063. [PubMed: 2719095]
50. Wang GL, Jiang BH, Rue EA, Semenza GL. Hypoxia-inducible factor 1 is a basic-helix-loop-helix-PAS heterodimer regulated by cellular O2 tension. Proc. Natl. Acad. Sci. 1995; 92:5510–5514. [PubMed: 7539918]
51. Schroedl C, McClintock DS, Budinger GR, Chandel NS. Hypoxic but not anoxic stabilization of HIF-1 requires mitochondrial reactive oxygen species. Am. J. Physiol. Lung Cell Mol. Physiol. 2002; 283:L922–L931. [PubMed: 12376345]
52. Sachs LA, Finkbeiner WE, Widdicombe JH. Effect of media on differentiation of cultured human tracheal epithelium. In Vitro Cell Dev. Biol. Anim. 2003; 39:56–62. [PubMed: 12892528]
53. Di Stefano A, Wittner M, Schlatter E, Lang HJ, Englert H, Greger R. Diphenylamine-2-carboxylate, a blocker of the Cl^--conductive pathway in Cl^{--}transporting epithelia. Pflugers Arch. 1985; 405(Suppl 1):S95–100. [PubMed: 2418410]
54. Fischer H, Schwarzer C, Illek B. Vitamin C controls the cystic fibrosis transmembrane conductance regulator chloride channel. Proc. Natl. Acad. Sci. USA. 2004; 101:3693–3696.
55. Lee MC, Penland CM, Widdicombe JH, Wine JJ. Evidence that Calu-3 human airway cells secrete bicarbonate. Am. J. Physiol. Lung Cell. Mol. Physiol. 1998; 274:L450–453.
56. Devor DC, Bridges RJ, Pilewski JM. Pharmacological modulation of ion transport across wild-type and ΔF508 CFTR-expressing human bronchial epithelia. Am. J. Physiol. Cell Physiol. 2000; 279:C461–479. [PubMed: 10913013]
57. Hudson VM. Rethinking Cystic fibrosis pathology: the critical role of abnormal reduced glutathione (GSH) transport caused by CFTR mutation. Free Radic. Biol. Med. 2001; 30:1440–1461. [PubMed: 11390189]
58. Ballatori N, Hammond CL, Cunningham JB, Krance SM, Marchan R. Molecular mechanisms of reduced glutathione transport: role of the MRP/CFTR/ABCC and OATP/SLC21A families of membrane proteins. Toxicol. Appl. Pharmacol. 2005; 204:238–255. [PubMed: 15845416]
59. Velsor LW, Kariya C, Kachadourian R, Day BJ. Mitochondrial oxidative stress in the lungs of cystic fibrosis transmembrane conductance regulator protein mutant mice. Am. J. Respir. Cell Mol. Biol. 2006; 35:579–86. [PubMed: 16763223]
60. Jones DP, Go YM, Anderson CL, Ziegler TR, Kinkade JM Jr, Kirlin WG. Cysteine/cystine couple is a newly recognized node in the circuitry for biologic redox signaling and control. FASEB J. 2004; 18:1246–1248. [PubMed: 15180957]
61. Bjornberg O, Ostergaard H, Winther JR. Measuring intracellular redox conditions using GFP-based sensors. Antioxid. Redox Signal. 2006; 8:354–361. [PubMed: 16677081]
62. Aslund F, Berndt KD, Holmgren A. Redox potentials of glutaredoxins and other thiol-disulfide oxidoreductases of the thioredoxin superfamily determined by direct protein-protein redox equilibria. J. Biol. Chem. 1997; 272:30780–30786. [PubMed: 9388218]

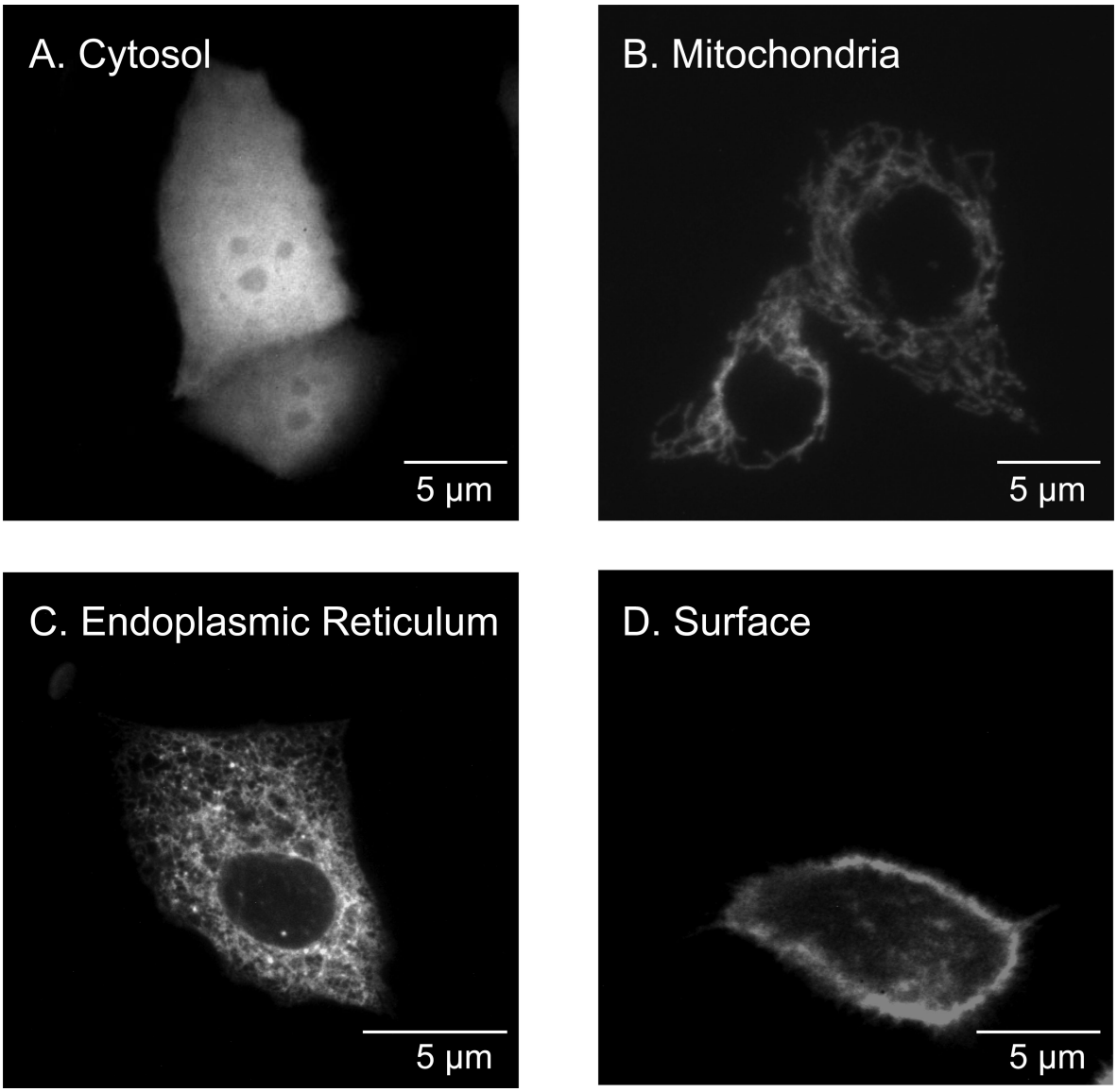

Fig. 1. Expression patterns of roGFP1 in (A) cytosol, (B) mitochondria, (C) ER, and (D) outside surface of plasma membrane of airway cells

CF15 cells were transiently transfected with organelle-specific roGFP1 plasmids. Confocal images were taken 48 hours post transfection (excitation, 488 nm; emission, 510 nm) on living cells in PBS containing 0.5 mM DTT to increase brightness at 488 nm.

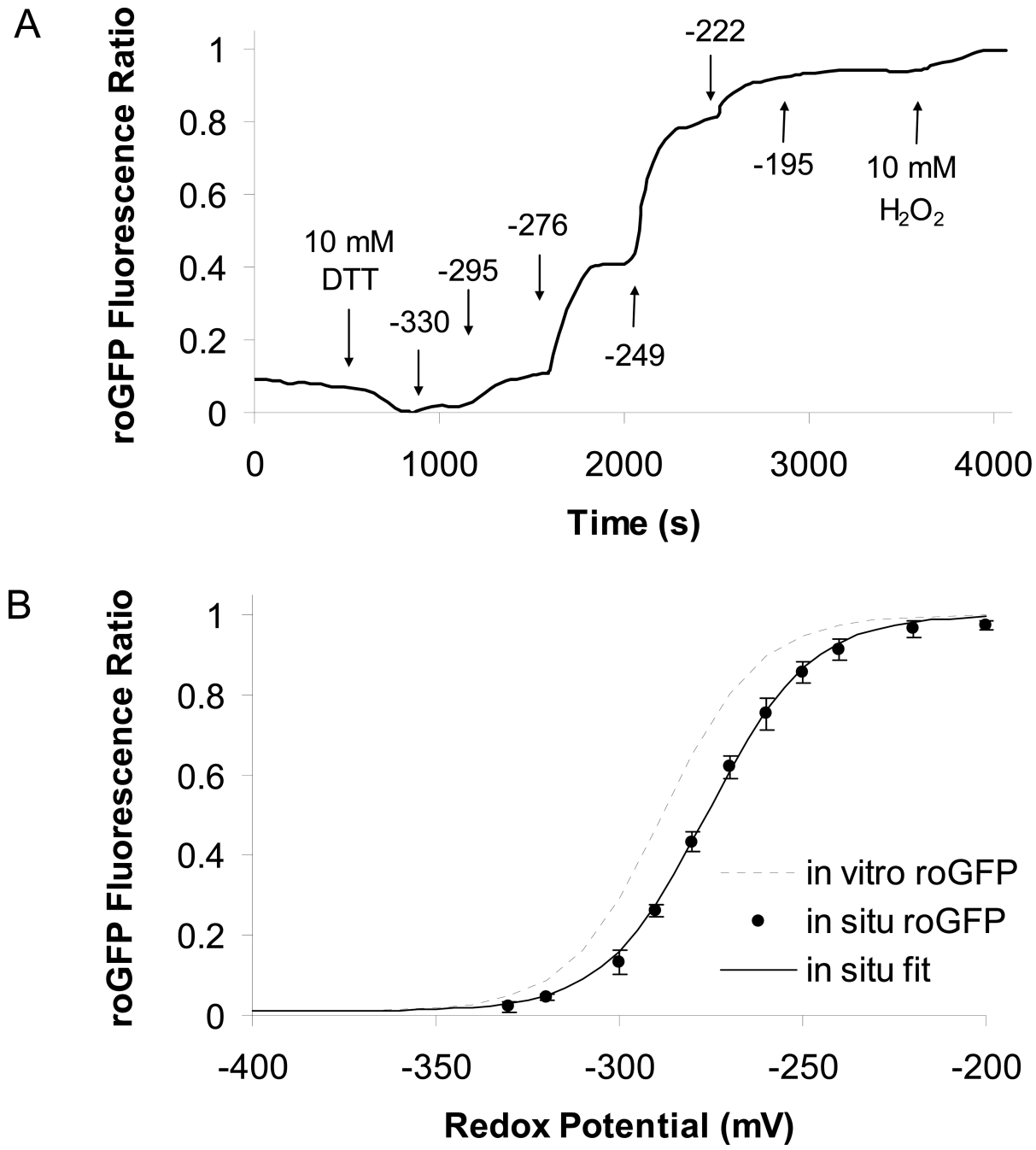

Fig. 2. Calibrating roGFP1 ratio in living cells

A. CF15 cells expressing roGFP1 were treated with 5 μg/ml digitonin for 10 minutes to permeabilize cell membranes to DTT and other small molecules. Then the cells were treated as shown by the arrows with 10 mM DTT_{red} (to attain 100% reduction), then with DTT_{red}:DTT_{ox} solutions (final concentration of DTT_{red}+DTT_{ox} ≥ 10 mM in Ringer's) that had redox potentials (in mV, calculated according to equation 1) shown above the arrows and finally with 10 mM H_2O_2 (to attain 100% oxidation of roGFP1). Resulting roGFP1 385/474 excitation ratios were background-subtracted and normalized (ratio with 10 mM DTT_{red} = 0% and ratio with 10 mM H_2O_2 = 100% oxidation) and plotted vs. time. Results

are typical of 8 similar experiments. **B.** Average roGFP1 ratios (●) from eight experiments like that in Fig. 2A were plotted vs. redox potential and fit by nonlinear regression (line) to f= y0+a/(1+exp(-(x-x0)/b)); y0=0.01, a=0.99, x0=-276, b=14). The *in vitro* calibration for recombinant roGFP1 performed by Hanson *et al* (2004) is shown for comparison (dotted line).

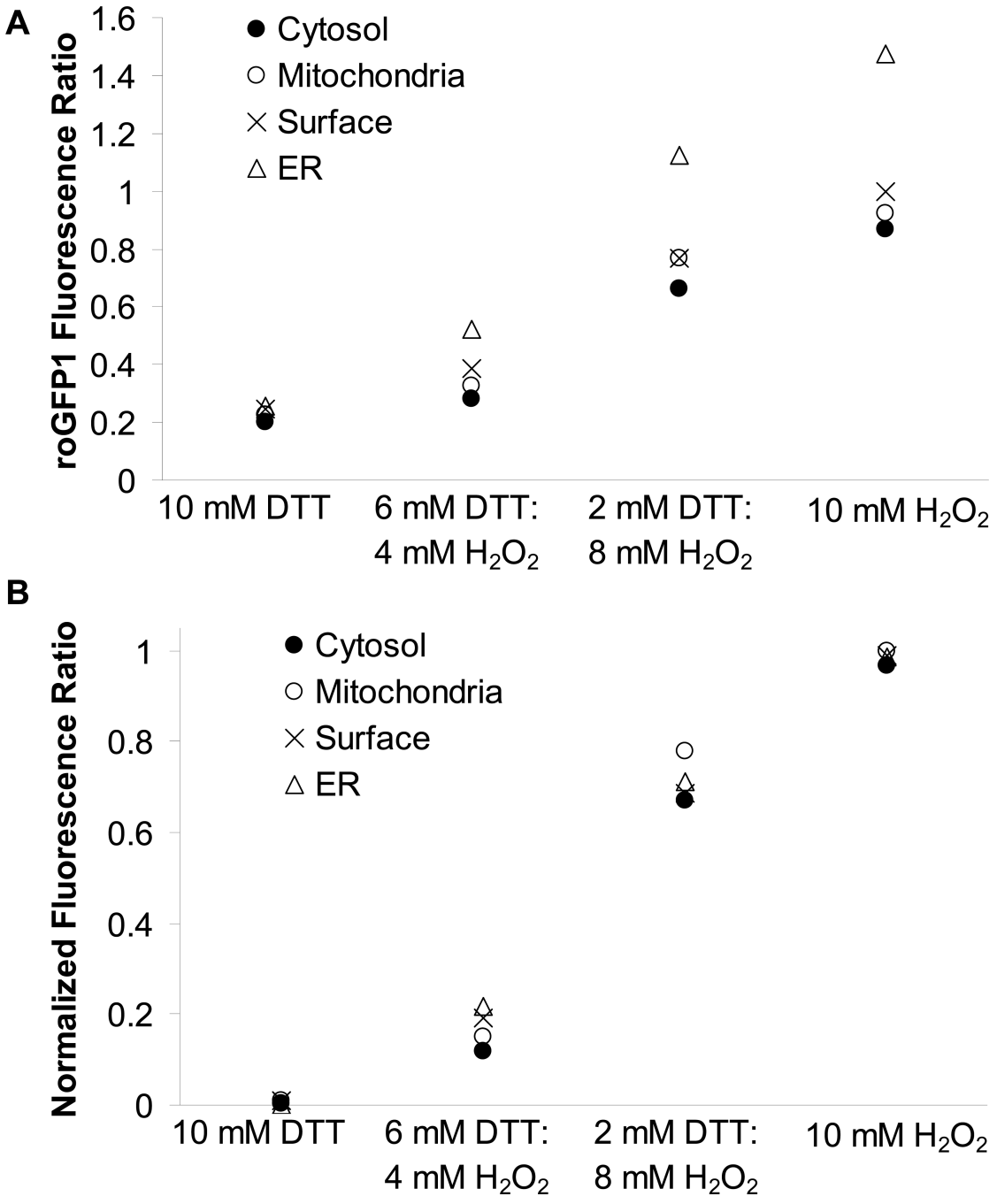

Fig. 3. Fluorescence properties of organelle-roGFP1

A. CF15 cells expressing cytosolic, mitochondrial, ER and cell surface roGFP1 were treated with solutions containing DTT_{red} and H_2O_2 at varying ratios (final concentration 10 mM in Ringer's). 385/474 nm fluorescence ratios for each compartment were recorded and background-subtracted (● cytosol, ○ mitochondria, × surface and ▲ ER; mean of n = 6 experiments shown, respectively), **B.** Normalization of data in Fig. 3A to maximal reduction and oxidation of roGFP1 fluorescence ratios show redox-sensing properties of roGFP1 were very similar for each organelle roGFP1.

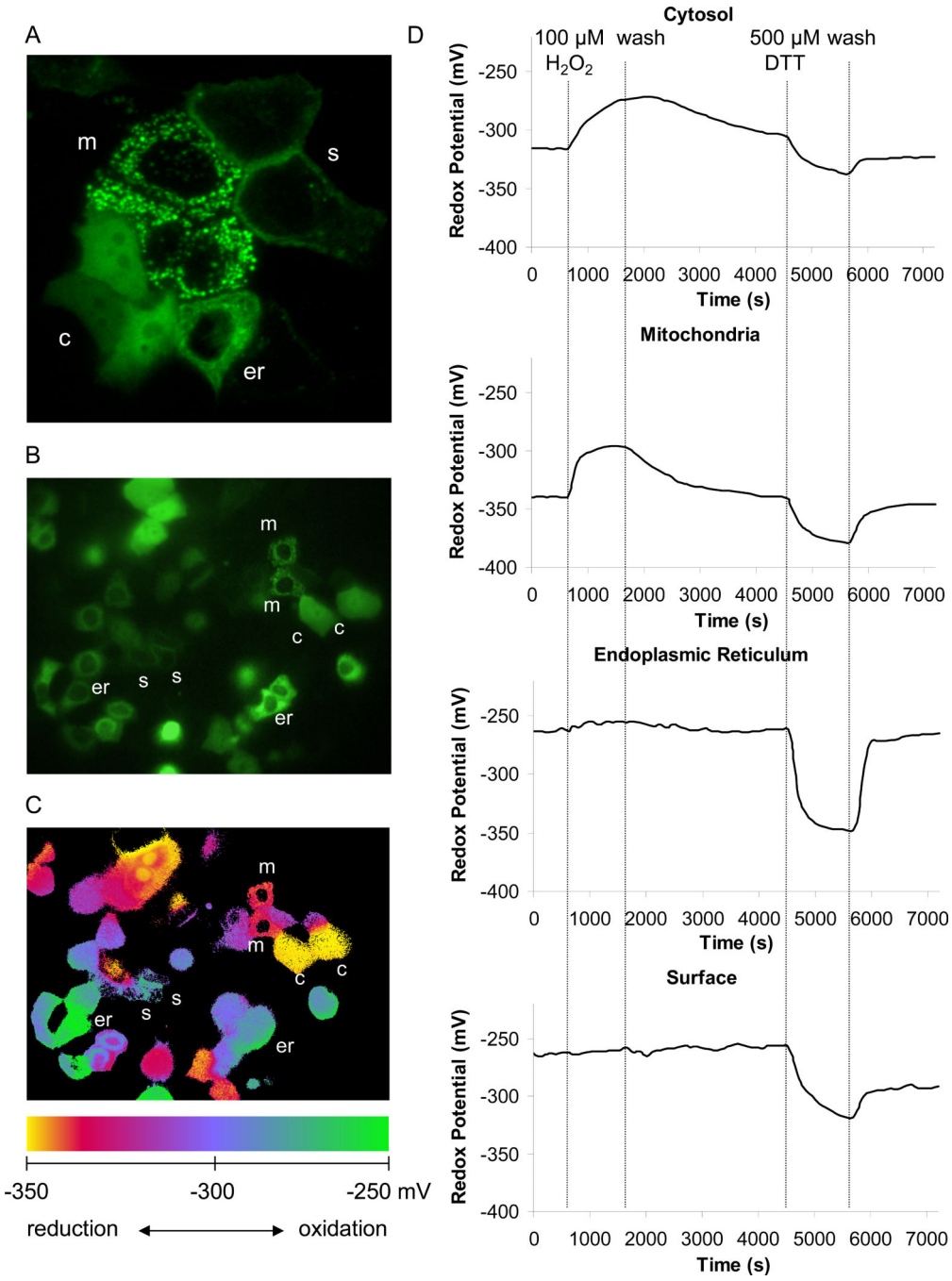

Fig. 4. Airway epithelia cells actively recover from transient oxidation or reduction

A. Confocal image of CF15 cells expressing four organelle-targeted roGFP1's in different cells on one cover slip, three cells expressed roGFP1 in the cytosol (denoted as c), one cell expressed in the ER (er), two cells expressed in the surface (plasma) membrane (s) and three cells expressed in the mitochondria (m). Cells were transfected onto one cover slip and examined after 24 hrs. **B.** Fluorescence microscopy of roGFP1 expressing cells excited at 385 nm for a typical field of cells on one cover slip. **C.** The roGFP1 385/474 excitation ratios for the same cells are shown as pseudo colors, with scale shown at the bottom of the

figure. **D.** Redox responses of organelle-targeted roGFP1's were tested by treating cells with 100 μM H_2O_2 or 500 μM DTT, and each recovery was monitored after washing cells with Ringer's solution. Raw data were background subtracted, calibrated into redox potentials, and displayed as pseudo colors. Data show averages of 2 - 6 cells for each organelle. Experiment typical of 10 similar experiments.

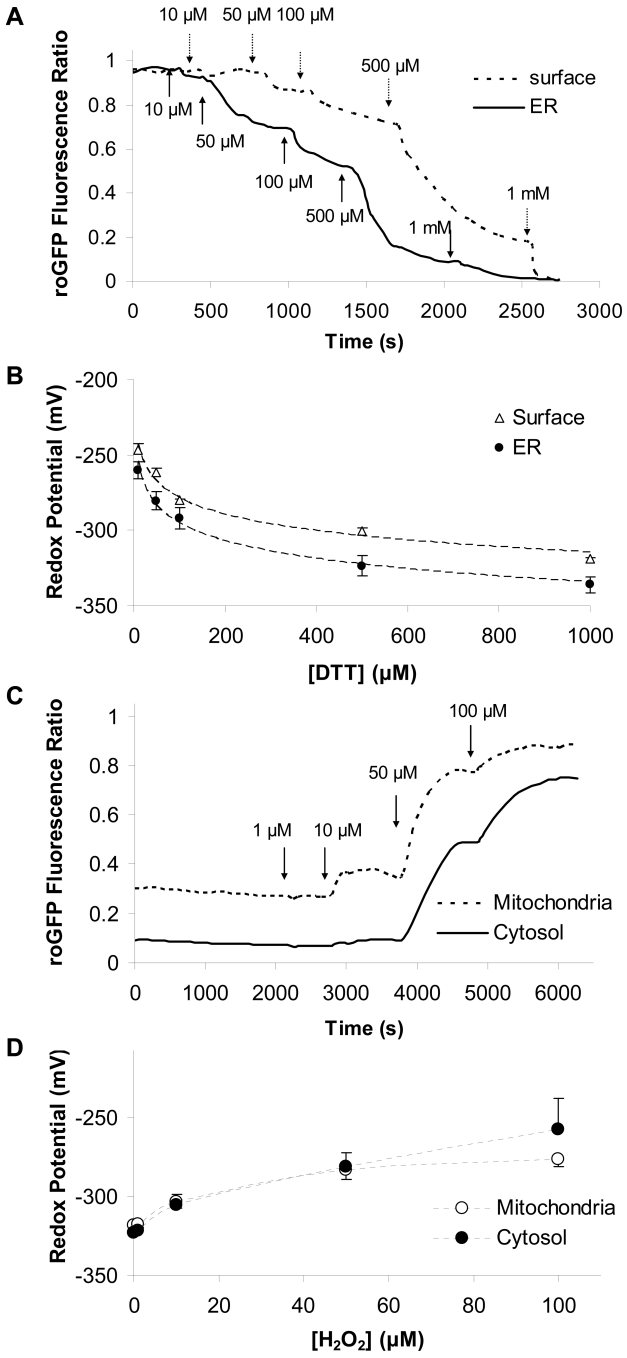

Fig. 5. Dose-dependent effects of DTT and H_2O_2 on redox potentials in the ER, surface, cytosol and mitochondria

A. Cell surface and ER roGFP1 ratios were measured during exposure of cells to increasing [DTT] (10 to 1000 µM, additions shown by arrows). **B.** Background-subtracted, normalized ratios for mitochondrial and cytosolic roGFP1 were calibrated, and redox potentials were plotted against [DTT]. Data were then fit (dotted line) using redox potentials measured at 10, 50, 100, 500 and 1000 µM DTT by the equation y= a*ln(x)+y0. The intercept of this fitted line at 0 µM DTT suggests a redox potential of -217 mV in the ER and -206 mV at the

cell surface. **C.** Mitochondrial and cytosolic roGFP1 ratios were measured during exposure of CF15 cells to increasing [H_2O_2] (1 to 100 μM, additions shown by arrows). **D.** Background-subtracted cytosolic and mitochondrial roGFP1 ratios were calibrated, and redox potentials were plotted as a function of [H_2O_2].

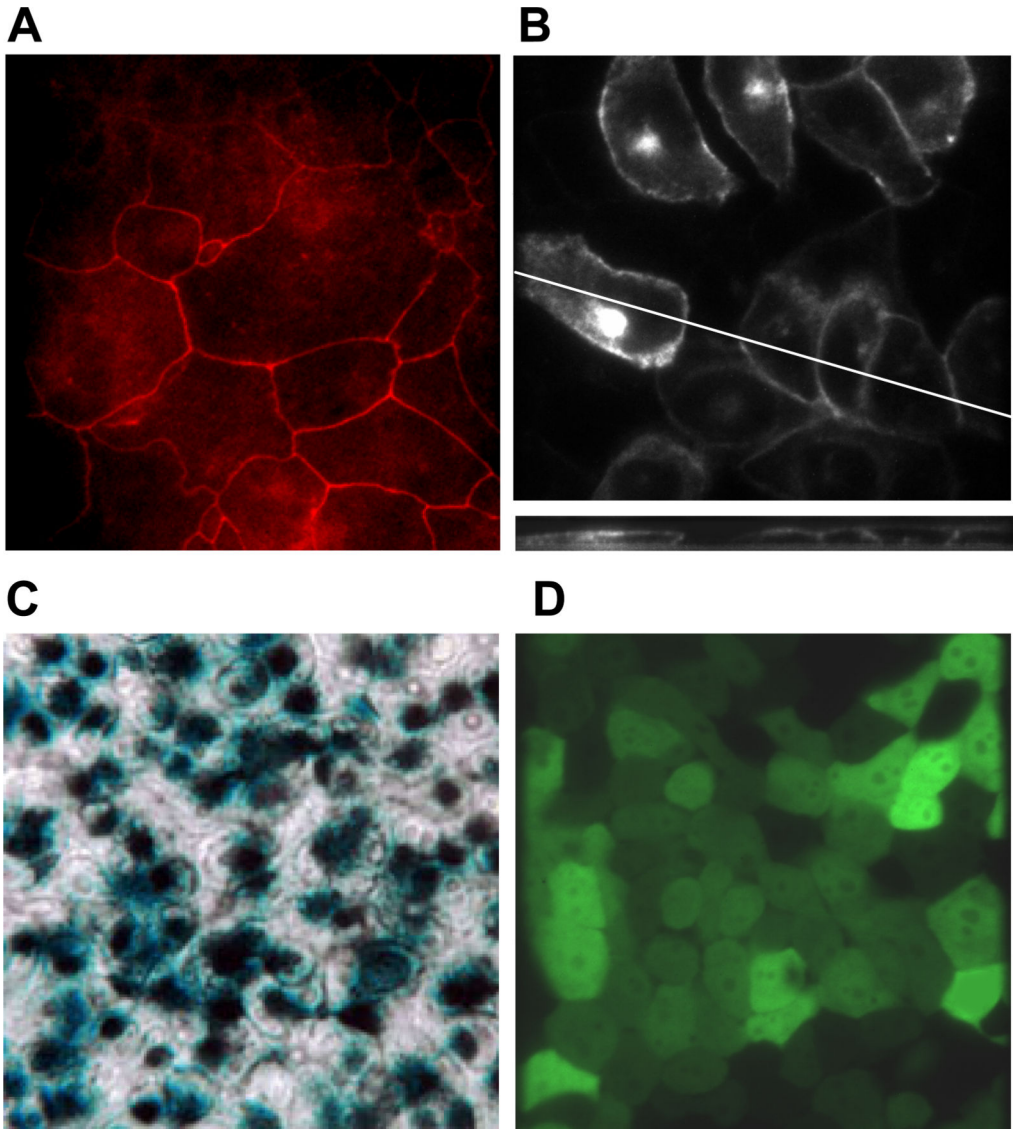

Fig. 6. Tight junctions, CFTR localization and adenoviral infections of CF15 cells

A. ZO-1 staining of fixed CF15 cells grown as a monolayer indicates the presence of tight junctions and their position around the apical regions of cells. **B.** CFTR localizes to the apical pole of CF15 cells grown on cover glasses. CF15 cells were grown on cover glasses, infected with CFTR-GFP adenovirus and localization was analyzed after 24 hours by confocal microscopy. The upper panel shows a representative XY scan close to the apical membrane. The lower section represents a XZ scan at 0.5 μm increments. **C.** Xgal staining demonstrates success of viral infection. CF15 cells were grown on filters and infected with lacZ-adenovirus (100 MOI) for 48 hrs (apical and basolateral surfaces). Cells were fixed, treated with 1 mg/ml xgal and incubated for 18 hrs at 37° C. The light microscopy image acquired using Nomarski optics (40 × objective) shows a representative field of six independent experiments. **D.** EGFP-adenovirus confirms infection efficiency. CF15 cells were grown on cover glasses and infected with EGFP-adenovirus (100 MOI) for 12 hours.

Confocal image was taken 24 hours post infection on cells grown to complete confluency (excitation 488 nm, 40× objective).

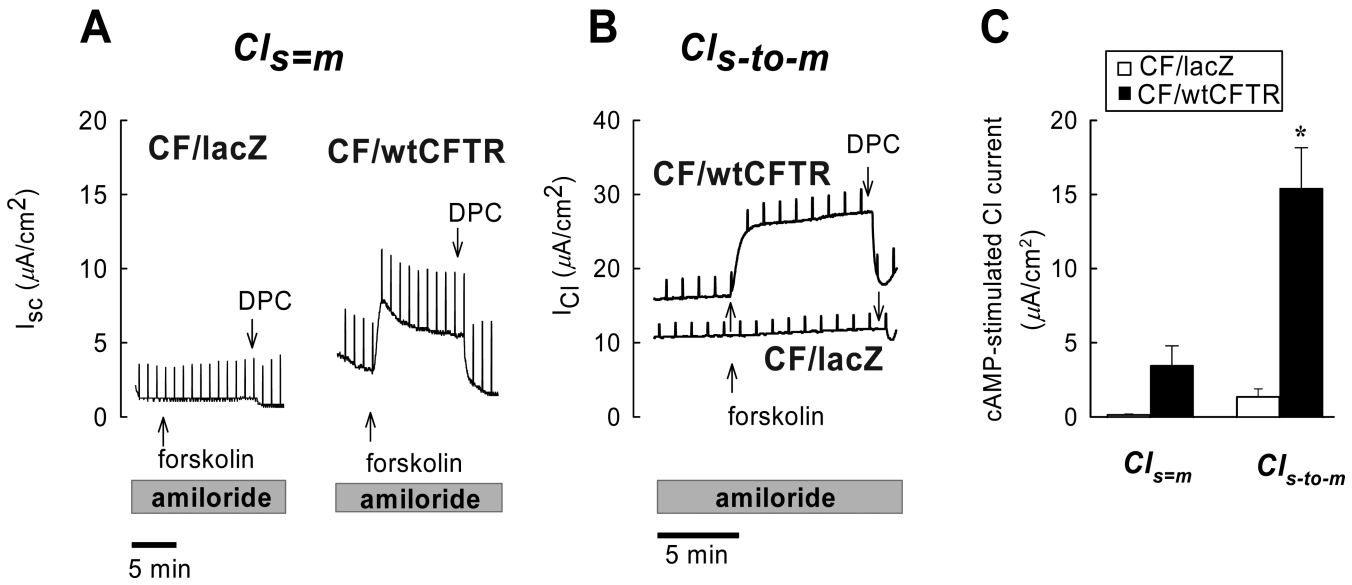

Fig. 7. Adenovirus-mediated gene transfer of CFTR corrects cAMP-stimulated Cl^-secretion across CF epithelia

Transepithelial Cl^- secretion was studied under short-circuit conditions in symmetrical solutions ($Cl_{s=m}$) and in the presence of a serosal-tomucosal Cl^- gradient ($Cl_{s\text{-}to\text{-}m}$) using CF15 epithelia expressing βgal (CF15-lacZ) or wild type CFTR (CF15-CFTR). Experiments were performed in the continuous presence of amiloride (20 μM) to block ENaC-mediated Na^+ currents. **A.** Serosal addition of forskolin (20 μM) stimulated Cl^- secretion across CF15-CFTR monolayers but not in CF15-lacZ controls. Addition of the Cl^- channel blocker DPC (5 mM, apical) effectively inhibited forskolin-stimulated Cl^- secretion. **B.** Removal of Cl^- from the apical solution increased forskolin-stimulated Cl^- currents and its subsequent inhibition by DPC. There was a very small inhibitory effect of DPC in the CF15-lacZ control group which may have been due to inhibition of residual ΔF508CFTR activity or other non-CFTR Cl^- conductances. **C.** Summary of forskolin-stimulated Cl^- currents. Average values are shown as mean ± SD, n= 3 - 10 experiments; * denotes statistically different from βgal control group (unpaired t-test, $p<0.05$).

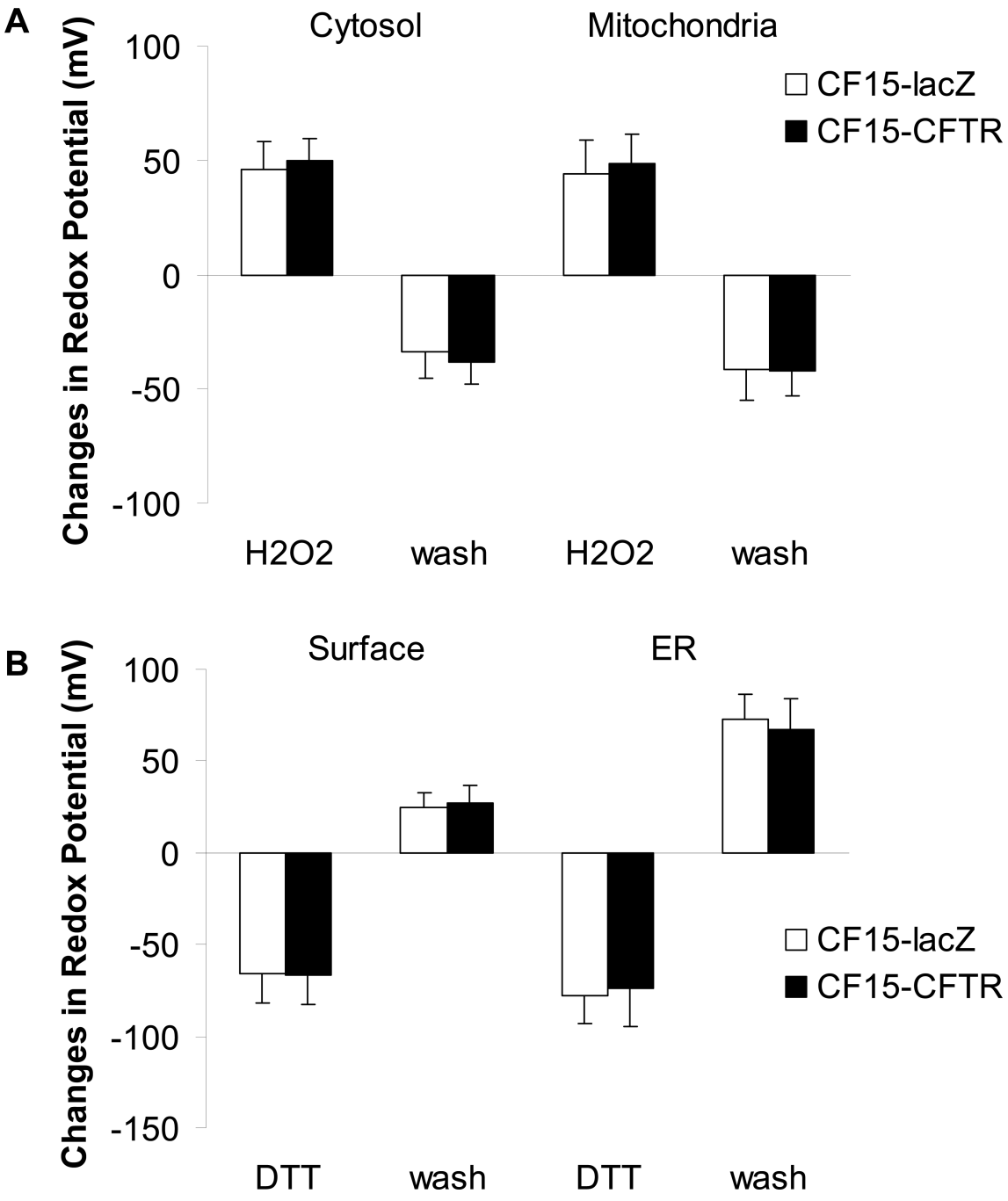

Fig. 8. CFTR does not affect redox potentials of cytosol, mitochondria, cell surface or ER upon H_2O_2 or DTT treatment

CF15 cells expressing cytosolic or mitochondrial roGFP1 (**A**) and cell surface or ER roGFP1 (**B)** were analyzed 48 h post adenoviral CFTR/lacZ infection. Steady state redox potentials were recorded at the beginning of each experiment and after addition of 100 μM H_2O_2 (for the cytosol and mitochondria in A) or 500 μM DTT (for the cell surface and ER in B). Recovered redox potentials were recorded one hour after removal of H_2O_2 or DTT by washing cells with Ringer's solution. Shown are differences in redox potential obtained by

subtracting initial or recovered redox potential values from those recorded after H_2O_2 or DTT treatment. Mean ± SD, n = 10.

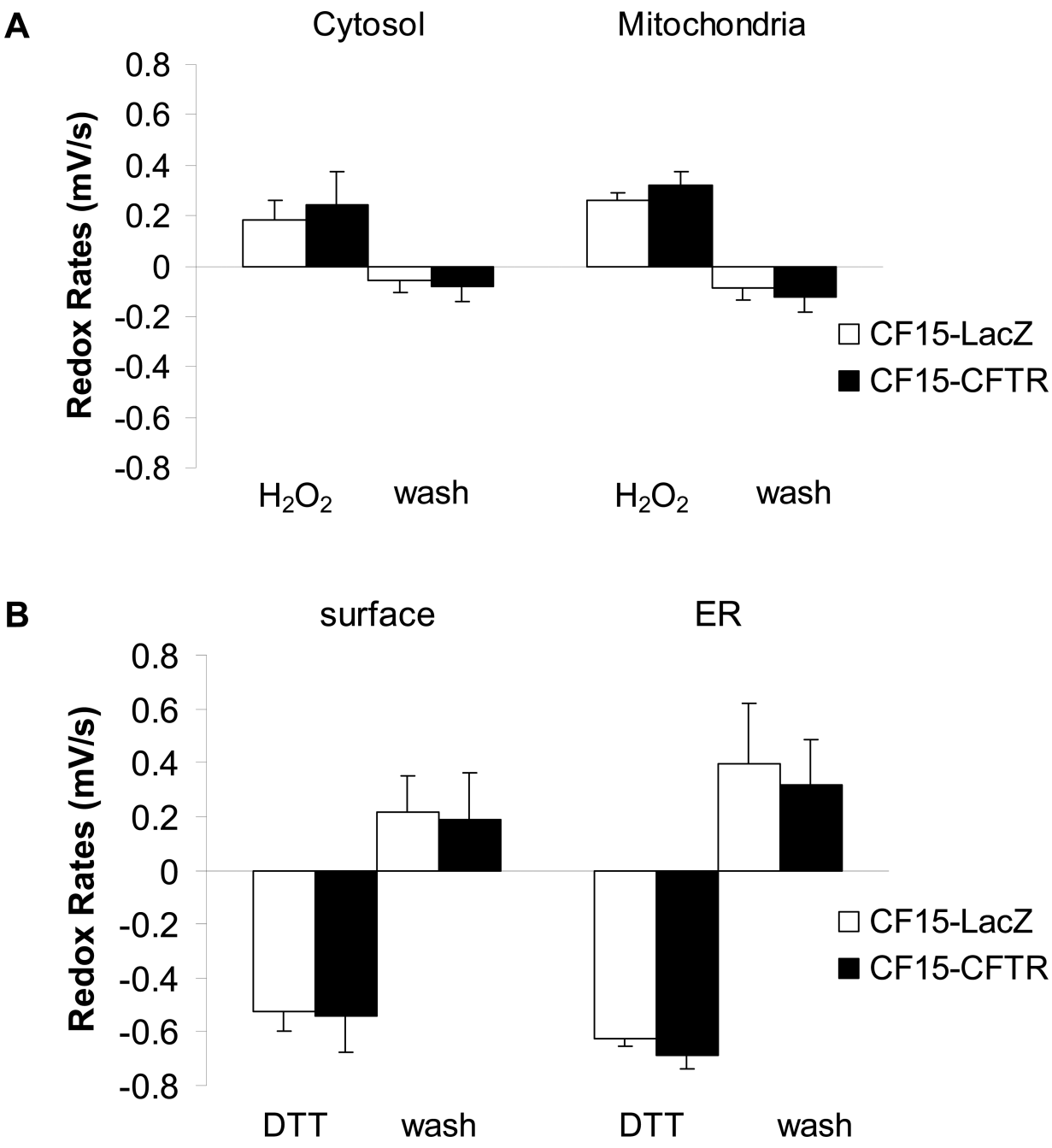

Fig. 9. CF15-lacZ and CF15-CFTR do not differ significantly in their rates of recovery from oxidative or reductive challenge

CF15 cells expressing cytosolic, mitochondrial, ER or cell surface roGFP1's were analyzed 24 h post transfection + adenoviral CFTR/lacZ infection. Cells were treated with 100 μM H_2O_2 or 500 μM DTT and each recovery was monitored after washing cells with Ringer's solution. Initial rates of recovery from oxidation or reduction were obtained by linear regression of time courses. Mean ± SD, n = 10.

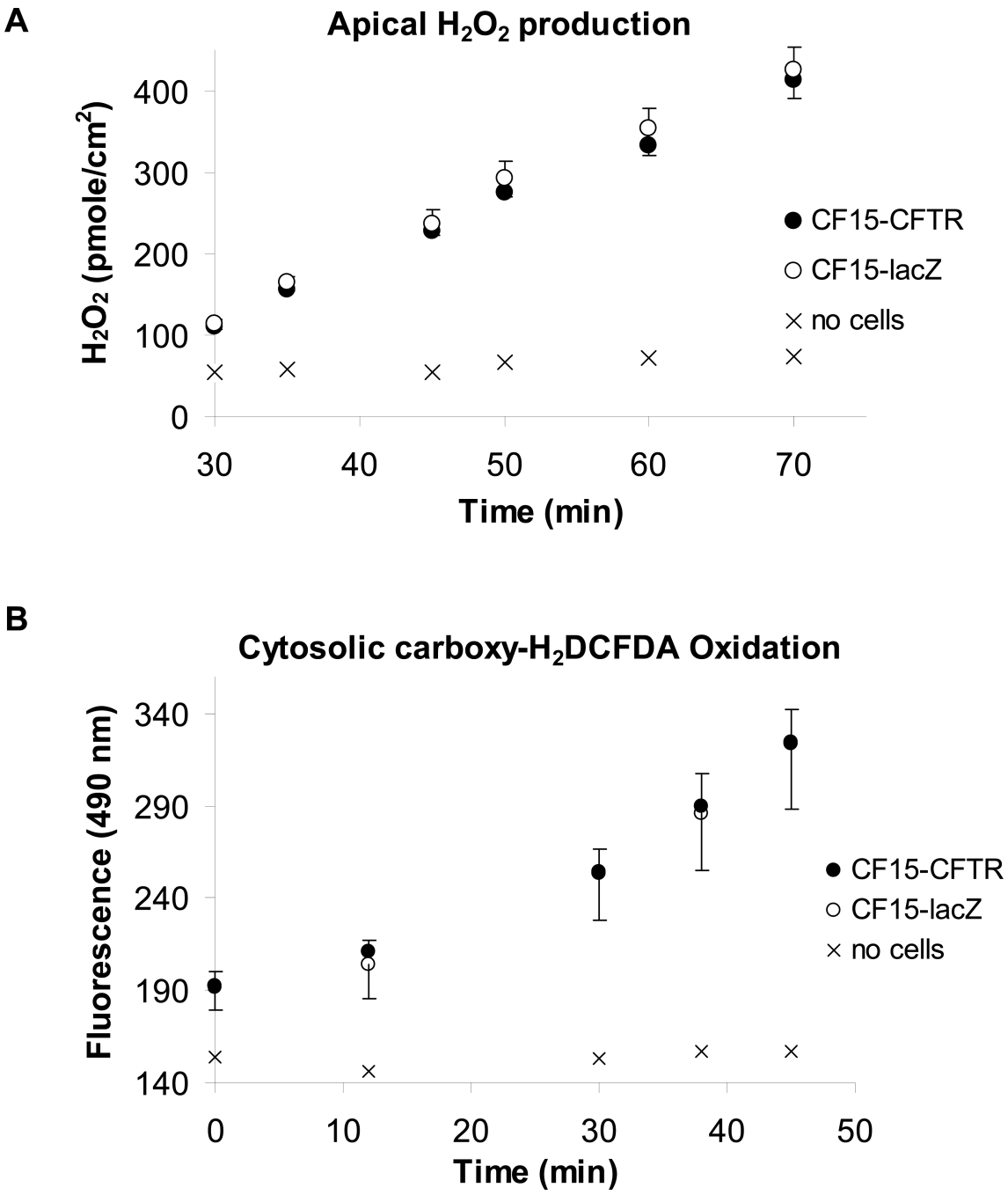

Fig. 10. Similar production of apical H_2O_2 and intracellular oxidation in CF15-CFTR- and CF15-lacZ cells

Accumulation of H_2O_2 assayed by HRP-dependent oxidation of Amplex Red at the apical side (**A**) and oxidation measured by oxidation of carboxy-H_2DCFDA in the cytosol (**B**) of CF15-lacZ and CF15-CFTR cells grown on permeable supports.

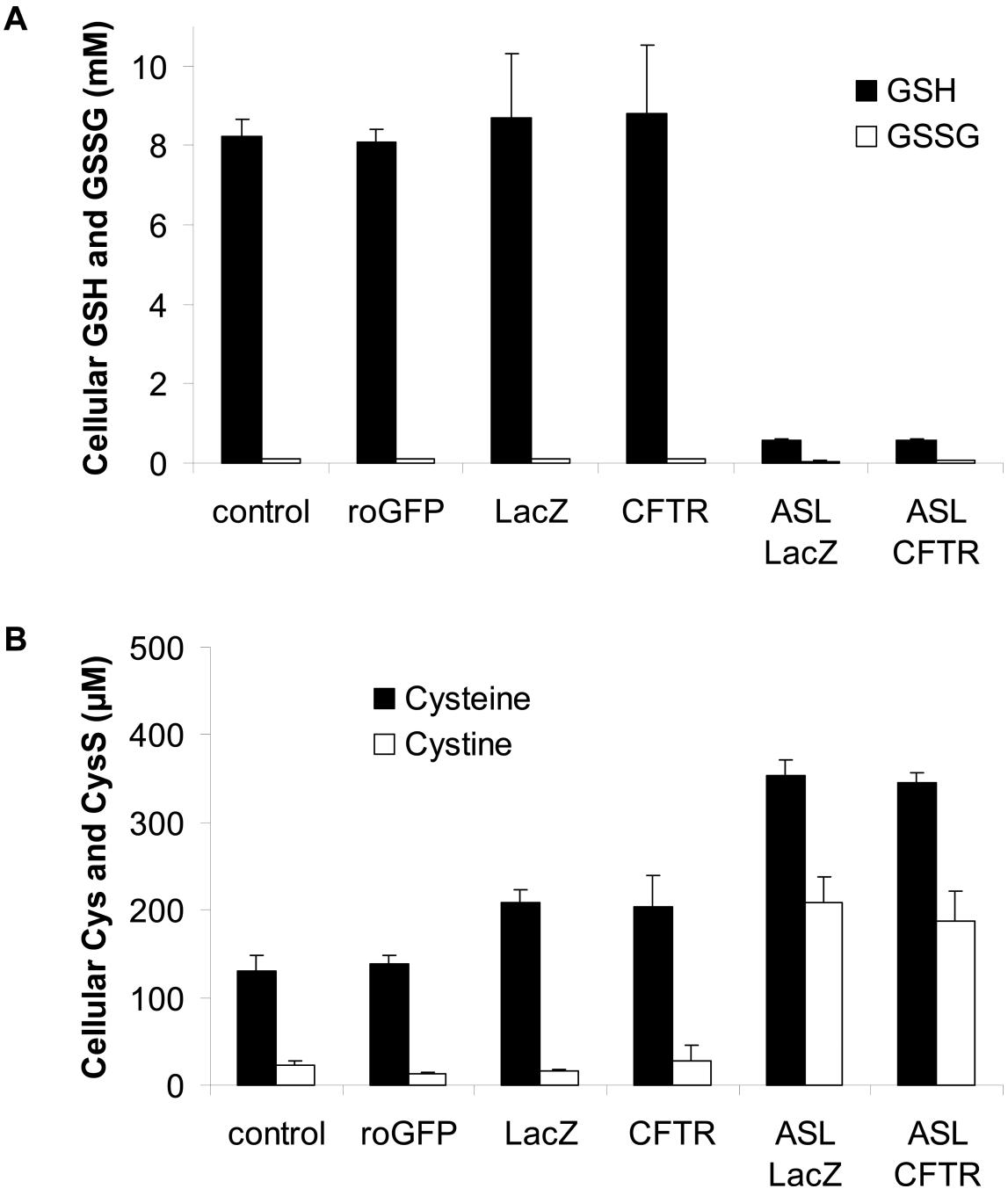

Fig. 11. GSH, GSSG, cysteine and cystine levels in cell lysates and apical secretion do not differ in CF15-lacZ and CF15-CFTR cells

HPLC analysis of small redox-active molecules was performed on cell lysates of CF15 cells grown in tissue culture dishes and untreated, transfected with roGFP1 or infected with either Ad-lacZ or Ad-CFTR. Measurements on surface liquid was performed on cells grown on permeable supports and infected with Ad-lacZ or Ad-CFTR. **A.** Concentration of GSH and GSSG were detected by HPLC and are expressed as absolute concentration after adjustment

to cell volume and dilution factor. The simultaneously performed analysis of cysteine and cystine from the same samples as in **A** is shown in **B**, Mean ± SD, n= 3.

Table 1

Redox potentials in resting cells at the beginning of experiments.

Cytosol	**CF15-lacZ**	**CF15-CFTR**	**Hela**
initial redox (mV)	−322	−320	−329
± SD	7	7	9
% oxidized	17.8	18.9	9.9
% reduced	82.2	81.1	90.1
Mitochondria	**CF15-lacZ**	**CF15-CFTR**	**Hela**
initial redox (mV)	−344	−345	−372
± SD	9	9	6
% oxidized	34.0	33.2	6.7
% reduced	66.0	66.8	93.3
Cell Surface	**CF15-lacZ**	**CF15-CFTR**	**CF15**
initial redox (mV)	−250	−250	−207 (a)
± SD	16	15	8
% oxidized	95.1	95.4	
% reduced	4.9	4.6	
ER	**CF15-lacZ**	**CF15-CFTR**	**CF15**
initial redox (mV)	−255	−256	−217 (a)
± SD	10	14	1
% oxidized	94.9	93.7	
% reduced	5.1	6.3	

(a) extrapolated potentials according to Fig. 5 roGFP1 fluorescence ratios were background-subtracted and normalized to minimal and maximal oxidation of the sensor. Ratios were converted to redox potentials using the *in situ* calibration described in Fig. 2B and values were then corrected for organelle pH.

Table 2

Redox potentials calculated from GSH:GSSG and cysteine:cystine concentrations in CF15 cells, roGFP1-expressing CF15, Ad-LacZ- and Ad-CFTR- infected CF15 cells.

	GSH mV ± SD	Cys mV ± SD
control	−257 ± 11	−156 ± 4
roGFP	−259 ± 3	−167 ± 2
CF15-lacZ	−261 ± 5	−172 ± 2
CF15-CFTR	−260 ± 5	−167 ± 7
apical CF15-lacZ	−202 ± 8	−153 ± 1
apical CF15-CFTR	−194 ± 6	−154 ± 2